A Feed-Forward Mechanosignaling Loop Confers Resistance to Therapies Targeting the MAPK Pathway in BRAF-Mutant Melanoma

Christophe Girard, Margaux Lecacheur, Rania Ben Jouira, Ilona Berestjuk, Serena Diazzi, Virginie Prod'Homme, Aude Mallavialle, Frédéric Larbret, Maeva Gesson, Sébastien Schaub, et al.

A feed-forward mechanosignaling loop confers resistance to therapies targeting the MAPK pathway in BRAF-mutant melanoma

C.A. Girard[1,2,$], M. Lecacheur[1,2,$], R. Ben Jouira[1,2,$], I. Berestjuk[1,2], S. Diazzi[1,2], V. Prod'homme[1,2], A. Mallavialle[1,2], F. Larbret[1,2], M. Gesson[3], S. Schaub[4], S. Pisano[5], S. Audebert[6], B. Mari[7], C. Gaggioli[5], E. Leucci[8,9], J.C. Marine[10,11], M. Deckert[1,2*], S. Tartare-Deckert[1,2*]

[1]Université Côte d'Azur, INSERM, C3M, Nice, France
[2]Equipe labellisée Ligue Contre le Cancer 2016, Nice, France
[3]Université Côte d'Azur, INSERM, C3M, Microscopy Facility,
[4] MICA facility, Université Côte d'Azur, CNRS, INSERM, IBV, Nice, France.
[5]Université Côte d'Azur, CNRS, INSERM, IRCAN, Nice, France
[6]Aix-Marseille University, CNRS, INSERM, Institut Paoli-Calmettes, CRCM, Marseille, France
[7]Université Côte d'Azur, CNRS, IPMC, Sophia Antipolis, France
[8]Laboratory for RNA Cancer Biology, Department of Oncology, KU Leuven, Leuven, Belgium
[9]TRACE, LKI Leuven Cancer Institute, KU Leuven
[10]Laboratory For Molecular Cancer Biology, VIB Center for Cancer Biology, VIB, Leuven, Belgium
[11]Department of Oncology, KU Leuven, Leuven, Belgium
[$]Co-first authors
*Co-last authors

Running title: Targeted therapies mechanically reprogram melanoma cells

Keywords: melanoma, extracellular matrix, YAP, MRTF, targeted therapies, resistance

Conflict of interest. The authors declare no potential conflicts of interest.

Financial support: This work was supported by funds from Institut National de la Santé et de la Recherche Médicale (Inserm), Ligue Contre le Cancer, Institut National du Cancer (INCA_12673), Fondation ARC, ITMO Cancer Aviesan (Alliance Nationale pour les Sciences de la Vie et de la Santé, National Alliance for Life Science and Health) within the framework of the Cancer Plan, and the French Government (National Research Agency, ANR) through the ''Investments for the Future'' LABEX SIGNALIFE: program reference # ANR-11-LABX-0028-01. We also thank financial supports by Conseil général 06 and Canceropôle PACA. R.B.J. was a recipient of a doctoral fellowship from Fondation ARC. I.B. was a recipient of a doctoral fellowship from La Ligue Contre le Cancer.

Corresponding Authors: Sophie Tartare-Deckert tartare@unice.fr and Marcel Deckert deckert@unice.fr, Inserm UMR1065/C3M, 151 Route de Ginestière BP2 3194, F-06204 Nice cedex 3.

ABSTRACT

Aberrant extracellular matrix (ECM) deposition and stiffening is a physical hallmark of several solid cancers and is associated with therapy failure. BRAF-mutant melanomas treated with BRAF and MEK inhibitors almost invariably develop resistance that is frequently associated with transcriptional reprogramming and a de-differentiated cell state. Melanoma cells secrete their own ECM proteins, an event that is promoted by oncogenic BRAF inhibition. Yet, the contribution of cancer cell-derived ECM and tumor mechanics to drug adaptation and therapy resistance remains poorly understood. Here, we show that melanoma cells can adapt to targeted therapies through a mechanosignaling loop involving the autocrine remodeling of a drug-protective ECM. Analyses reveal that therapy resistant cells associated with a mesenchymal de-differentiated state display elevated responsiveness to collagen stiffening and force-mediated ECM remodeling through activation of actin-dependent mechanosensors Yes-associated protein (YAP) and Myocardin-related transcription factor (MRTF). Short-term inhibition of MAPK pathway also induces mechanosignaling associated with deposition and remodeling of an aligned fibrillar matrix. This provides a favored ECM reorganization to promote tolerance to BRAF inhibition in a YAP and MRTF-dependent manner. Matrix remodeling and tumor stiffening are also observed *in vivo* upon exposure of *BRAF*-mutant melanoma cell lines or patient-derived xenograft models to MAPK pathway inhibition. Importantly, pharmacological targeting of YAP reverses treatment-induced excessive collagen deposition, leading to enhancement of BRAF inhibitor efficacy. We conclude that MAPK pathway targeting therapies mechanically reprogram melanoma cells to confer a drug-protective matrix environment. Preventing melanoma cell mechanical reprogramming might be a promising therapeutic strategy for patients on targeted therapies.

SIGNIFICANCE

These findings reveal a biomechanical adaptation of melanoma cells to oncogenic BRAF pathway inhibition, which fuels a YAP/MRTF-dependent feed-forward loop associated with tumor stiffening, mechanosensing and therapy resistance.

INTRODUCTION

Reciprocal feedback between the ECM and tumor cells influence the hallmarks of cancer by providing biological abilities to malignant cells that are required for growth, survival and dissemination. The ECM is a dynamic network of macromolecules with distinctive biochemical and mechanical properties that plays a major role in establishing tumor niches (1). Increased ECM deposition, fiber alignment and covalent cross-link between collagen molecules lead to tumor stiffening, which has been associated to an elevated risk of cancer and poor clinical outcome in patients with breast or pancreatic cancers (2,3).

Cancer-associated fibroblasts (CAFs) are the main producers of tumorigenic ECM and function like myofibroblasts during wound healing and fibrosis (4). Cells apply contractile forces to sense the physical environmental stiffness through integrin-based focal adhesion (FA) complexes that connect the actin-myosin cytoskeleton with the ECM (2,5). Matrix rigidity also leads to enhanced nucleus localization and activity of the mechanical-responsive YAP transcriptional regulator of the Hippo pathway (6). In CAFs, YAP acts as a critical factor regulating force-mediated ECM remodeling towards increased stiffening (7). Similar to YAP, the SRF transcriptional co-activator MRTF is translocated to the nucleus upon actin polymerization and functionally interacts with YAP to coordinate mechanosignaling and CAF contractility (8,9). Beside, YAP mainly through its interaction with TEAD transcription factors have been shown to promote resistance to RAF/MEK–targeted cancer therapies in tumor cells such as melanoma (10-12).

Because of its resistance to treatment and propensity for metastasis, cutaneous melanoma is one of the most aggressive human cancers (13). Melanoma comprises phenotypically heterogeneous subtypes of cancer cells that can switch between transcriptional programs and differentiation states (14-16). The majority of human melanomas display genetic alterations in *BRAF* or *NRAS*, leading to constitutive activation of the MAP Kinase (MAPK) pathway. MAPK pathway inhibitors, such as BRAF inhibitors (BRAFi), MEK inhibitors (MEKi), or their combination, achieve significant clinical benefits in patients with BRAFV600-mutant melanoma. However, most patients relapse within months due to the acquisition of drug resistance attributed to intrinsic genetic and non-genetic changes in melanoma cells. While genetic resistance frequently result from the reactivation of the MAPK pathway through *de novo* mutations, such as *NRAS* mutations (17,18), non-genetic mechanisms involve epigenetic and/or transcriptomic changes in tumor cells during the early phase of treatment (19,20).

Such mechanisms often result in a de-differentiation cell state characterized by down-regulation of the master regulator of melanocyte differentiation Microphthalmia-Associated Transcription Factor (MITF) and up-regulation of receptor tyrosine kinases (RTKs) such as AXL (21-23). In addition, the de-differentiated resistant $MITF^{low}/AXL^{high}$ population was shown to display a mesenchymal invasive phenotype (24-26). Transcriptional reprogramming of proliferative drug-sensitive melanoma cells into invasive drug-resistant cell population is thus a critical event in acquired resistance to targeted therapies.

Beside tumor cell-autonomous events, there is evidence that extrinsic factors derived from the tumor microenvironment contribute to melanoma resistance to MAPK pathway inhibition. Stromal cells including CAFs and macrophages secrete growth and inflammatory factors, and ECM components such as fibronectin, which contribute to drug tolerance (27-31). Interestingly, melanoma cells have the ability to secrete their own matrix, in particular upon cellular transition to a de-differentiated mesenchymal state occurring in response to MAPK pathway inhibition (20,32,33). In this study we asked whether melanoma cell-derived ECM impacts on tumor mechanics and contributes to resistance to targeted therapies. We show that both acquired resistance and early adaptation to MAPK signaling inhibition paradoxically induces a force-mediated ECM reprogramming in melanoma cells that increases cancer cell intrinsic mechanical sensing properties and alters ECM composition and topography. This fuels a mechanical positive-feedback loop where melanoma cell-derived ECM and YAP/MRTF intracellular pathways play a pivotal role and that could favor the reservoir of therapy-resistant cells.

MATERIALS AND METHODS

Cells and reagents. Melanoma cell lines 501Mel and MNT1 were obtained as described before (34,35). 1205Lu cells were from Rockland (USA). Isogenic pairs of Verumafenib-sensitive (P) and resistant (R) cells (M229, M238, M249) were provided by R. Lo (21). Cells were cultured in Dulbecco's modified Eagle Medium (DMEM) plus 7% FBS (Hyclone). Resistant cells were continuously exposed to 1 μM Vemurafenib. Cell lines were used within 6 months between resuscitation and experimentation. To guarantee cell line authenticity, cells were expanded and frozen at low passage after their receipt from original stocks, used for a limited number of passages after thawing and routinely tested for the expression of melanocyte-lineage proteins such as MITF. All cell lines were routinely tested for the absence of mycoplasma by PCR. For live imaging, M2380P, 501Mel and 1205Lu were transduced with NucLight Red lentivirus reagent (Essen Bioscience) and selected with puromycin (1 μg/ml). Culture reagents were purchased from Thermo Fisher Scientific. BRAFi (PLX4032, Vemurafenib), MEKi (GSK1120212, Trametinib) and ROCK inhibitor Y27632 were from Selleckem. YAP inhibitor Verteporfin was from Sigma.

RNAi studies. siGENOME siRNA SMARTpools for YAP1, MRTFa and nontargeting control were from Dharmacon (Horizon Discovery). 50 nM of either siRNA pool was transfected using Lipofectamine RNAiMAX (Thermo Fisher Scientific), following the manufacturer's protocol.

Immunoblot analysis and antibodies. Cell lysates were subjected to immunoblot analysis as described before (35). The following antibodies were used at dilution of 1:1,000, unless otherwise stated: Type I collagen and α-SMA (Abcam); TAGLN2 (Genetex); PDGFRβ (Cohesion Biosciences); EGFR and LOXL2 (Bio-Techne); LOX (Novus Biological); MITF (Thermo Fisher Scientific); fibronectin, thrombospondin (TSP1), β1 integrin, FAK, paxillin, FAP, and MRTF (BD Biosciences); SPARC (Haematologic Technologies); ERK1/2, HSP90, HSP60, MLC2 (Santa Cruz Biotechnology); AXL, YAP, phospho-Paxillin (Y118), phospho-ERK1/2 (T202/Y204), phospho-Rb (S807/811), Rb, p27KIP1, caveolin-1, survivin and tubulin (Cell Signaling Technology).

Real-time quantitative PCR. Gene expression levels were determined by RT-qPCR as described (34). Data were presented as relative gene expression according to the ΔΔCt

method. Heatmaps depicting fold changes of gene expression were prepared using MeV software. Primer sequences are available upon request.

Generation of cell-derived ECM and drug-protection assays. 3D ECMs were generated as previously described (36). Briefly, gelatin-coated culture dishes were seeded with cells and cultured for 8 days in complete medium, supplemented with 50 μg/ml ascorbic acid every 48 h. Cell cultures were then washed with PBS and matrices were denuded following a 2 min treatment with pre-warmed extraction buffer (PBS 0.5% Triton X-100, 20 μM NH_4OH). Matrices were then gently washed several times with PBS. For drug-protection assays, melanoma cells were seeded onto decellularized matrices for 24 h, and cultured for another 48 h period in presence or not of indicated drugs.

Cell proliferation. Cell cycle profiles were determined by flow cytometry as described before (34). Proliferation was measured by a MTS conversion assay (34) or followed by live imaging of NucLight Red-stained cells using the IncuCyte ZOOM™ system according to the manusfacturer's instructions (Essen BioScience) or by nuclei quantification of Hoescht-stained cells.

Cell contraction assay. 5×10^4 melanoma cells were embedded in 100 μl of collagen I/Matrigel and seeded on a glass bottom 96-well plate (MatTek). Once the gel was set (1 h at 37°C), cells were maintained in DMEM 10% FBS with or without indicated drugs. Gel contraction was monitored at day 3. The gel area was measured using ImageJ software and the percentage of contraction was calculated using the formula 100 × (well diameter−gel diameter)/well diameter as described (37).

Traction force microscopy (TFM). Contractile forces exerted by melanoma cells were assessed by TFM as described (38) using collagen-coated polyacrylamide hydrogels with shear modulus of 4kPa coated with red fluorescent beads (SoftTrac, Cell Guidance Systems). Cells were plated on fluorescent bead–conjugated gels for 48 h. Images were acquired before and after cell removal using a fluorescence microscope (Leica DMI6000, 10X magnification). Tractions exerted by cells were estimated by measuring beads displacement fields, computing corresponding traction fields using Fourier transformation and calculating root-mean-square traction using the particle image velocity plugin on ImageJ. The same procedure was performed on a cell-free region to measure baseline noise.

Immunofluorescence analysis. Cell were grown either on glass coverslips or collagen-coated polyacrylamide/bisacrylamide synthetic hydrogels with defined stiffness as described (39). Following treatment, cells were rinsed, fixed in 4% formaldehyde, and incubated in PBS 0.2% saponin 1% BSA in PBS for 1 h with 1:100 dilution of the indicated primary antibodies. Following incubation with AlexaFluor-conjugated secondary antibodies (1:1,000), coverslips and hydrogels were mounted in Prolong antifade (Thermo Fisher Scientific). F-actin was stained with Texas Red-X or AlexaFluor488 phalloidin (1:100, Thermo Fisher Scientific). Nuclei were stained with DAPI. Images were captured on a widefield microscope (Leica DM5500B, 40X magnification). The orientation of fibronectin fibers was assessed on immunofluorescence images using ImageJ software. Data were plotted as a frequency distribution.

Collagen imaging. Collagen fibers were stained using Picrosirius red accordingly to (40). Images were acquired under polarized illumination using a light transmission microscope (Zeiss Axio Observer, 5X magnification). Background signal was determined on each sample from an empty zone. Background was then subtracted from the signal emitted by the region of interest. A minimum of 3 background-subtracted samples was used for quantification. The area was calculated as followed: area of tumors was selected based on HE staining to exclude analysis of peritumoral regions. Images were then converted into gray scale pictures and the threshold option ''Minimum'' on the ImageJ software (https://imagej.nih.gov/ij/) was selected to quantify the area of collagen fibers and normalize it to the total area selected. Second harmonic generation (SHG) and multiphoton-fluorescence images were acquired on a Zeiss 780NLO (Carl Zeiss Microscopy) with Mai Tai HP DeepSee (Newport Corporation). Acquisitions were achieved simultaneously in backward through 10x dry NA 0.45 objective and forward through condenser NA 0.55. Each side is equipped with dual NDD GaAspP detectors (BiG) with 440/10 (for SHG forward and backward) and 525/50 filter (for autofluorescence). Transmission images were acquired with 514nm laser through the 525/50 filter.

Cell line-derived xenograft (CDX) tumor models. Mouse experiments were carried out in accordance with the Institutional Animal Care and the local ethical committee (CIEPAL-Azur agreement NCE/2014-179). 1×10^6 melanoma cells were subcutaneously implanted into both

flanks of 6 week old female athymic nude nu/nu mice (Envigo). When tumor reached 100 mm^3, mice were randomly grouped into control and test groups. The BRAFi group received 6 intraperitoneal injections of Vemurafenib (35 mg/kg) over a period of 2 weeks. Verteporfin was delivered intraperitoneally three times per week at 45 mg/kg. Mice in the control group were treated with vehicle. At the end of the experiment, mice were sacrificed, tumors were dissected, weighed, and either snap frozen in liquid nitrogen (for mRNA and protein analysis), in Tissue-Tek O.C.T. (VWR) (for AFM analysis) or formalin fixed and paraffin embedded for picrosirius red staining, SHG analysis and immunohistochemistry.

Patient-derived xenograft (PDX) tumor models. PDX models were developed by TRACE (PDX platform at the KULeuven University) and treated with the BRAFi-MEKi combination as described before (41) (see Supplementary Informations for details). Tumor biopsies were formalin-fixed and paraffin embedded in sections of about 5 µm for picrosirius red staining and immunohistochemistry.

Elastic modulus measurements. Mechanical properties of tumor sections were analyzed by atomic force microscopy (AFM) as described before (42) with a Bioscope Catalyst operating in Point and Shoot (Bruker Nano Surfaces), coupled with an inverted optical microscope (Leica DMI6000B, Leica Microsystems Ltd.). The apparent Young's Modulus (E_{app}) was measured on unfixed frozen tumor sections using a Borosilicate Glass spherical tip (5 µm of diameter) mounted on a cantilever with a nominal spring constant of 0.06 N/m (Novascan Technologies). The force-distance curves were collected using a velocity of 2 µm/s, in relative trigger mode and by setting the trigger threshold to 1 nN. E_{app} values were presented in a boxplot using GraphPad Prism (GraphPad software).

Gene Expression Omnibus (GEO) data analysis. Public datasets of human melanoma cell lines developing drug resistance to Vemurafenib (M229R and SKMel28R) and double resistance to Vemurafenib and Selumetinib (M229DDR and SKMel28DDR) were used to analyze gene levels compared to drug-naive parental cell lines (GSE65185) (19). Differential gene expression was also examined in datasets derived from tumor biopsies from melanoma patients before and after development of drug resistance to BRAFi, MEKi or BRAFi/MEKi combination (GSE50535 (25); Tirosh *et al.* Supplementary information (15)). Normalized data were prepared using MeV software.

Statistical analysis. Unless otherwise stated, all experiments were repeated at least three times and representative data/images are shown. Statistical data analysis was performed using GraphPad Prism 5 software. Unpaired two-tailed Mann-Whitney test were used for statistical comparisons between two groups and Kruskal-Wallis test with Dunn posttests or two-way analysis of variance test with Bonferroni post tests to compare three or more groups. Error bars are ± s.d.

RESULTS

MITF^{low}/AXL^{high} BRAFi-resistant cells display increased mechano-responsiveness and YAP/MRTF activation. To investigate whether acquired resistance to BRAFi modifies mechanosensing pathways, we exploited models of isogenic pairs of parental (P) and resistant (R) melanoma cells showing either reactivation of MAPK pathway through NRAS mutation (M249R) or upregulation of AXL, EGFR and PDGFRβ RTKs associated with low levels of MITF and reduced differentiation of melanoma cells (M229R, M238R) (Supplementary Fig. S1) (20,21). Cells were cultured on collagen-coated hydrogels with stiffness ranging from 0.2kPa (low), 4kPa (medium) to 50 kPa (high) (39). In contrast to parental sublines, a dramatic modification of M238R (Fig. 1A and B) and M229R (Supplementary Fig. S2A and B) cell morphology measured by actin reorganization, cell roundness and area was noticeable upon increased substrate stiffness. In contrast, the shape and actin cytoskeleton of the NRAS-mutated M249R subline and its parent M249P showed no significant changes in response to mechanical stimulation (Fig. 1C and 1D; Supplementary Fig. S2C and S2D). Importantly, mesenchymal BRAFi-resistant cells M229R and M238R, but not NRAS-mutated M249R cells, exhibited an enhanced capacity to proliferate on a collagen-coated stiff substrate (Fig. 1E and S2E).

The β1 integrin/FA pathway is essential for ECM mechanosignaling (43). Consistently, when compared to drug-sensitive cells, M238R and M229R cells expressed higher levels of β1 integrin and increased phosphorylation of FA components, including FAK, p130Cas and paxillin (Supplementary Fig. S1). In addition, M238R cells displayed higher number of FAs upon increased matrix rigidity compared to parental cells (Supplementary Fig. S3).

YAP and MRTF are critical transcriptional mediators of mechanical signals in mammalian cells through partially overlapping signaling pathways and target genes (6,7,9,44). Immunofluorescence analysis of melanoma cells plated on soft or rigid substrates revealed that in contrast to M238P cells, M238R cells showed higher levels of nuclear YAP (Fig. 2A) on low stiffness substrates. Nuclear YAP (Fig. 2A) and MRTF (Fig. 2B) markedly increased in M238R cells plated on medium and high substrate stiffness, while translocation of YAP and MRTF was only apparent when parental cells were plated on stiff substrate. Consistently, the expression of shared YAP/MRTF target genes paralleled increasing collagen rigidity in M238R, but not M238P cells (Fig. 2C). Furthermore, impairment of the actomyosin cytoskeleton with the ROCK inhibitor Y27632 reduced the nuclear localization of YAP and

MRTF in M238R cells grown on high stiffness substrate (Fig. 2D). Accordingly, ROCK inhibition abrogated the expression of two shared YAP/MRTF target genes *CTGF* and *CYR61* activated in M238R cells on stiff substrate (Fig. 2E).

Finally, to evaluate the potential contribution of ECM stiffness-induced YAP and MRTF activation in the mesenchymal resistant phenotype, M238R cells cultured on rigid collagen hydrogels were transfected with siRNA pool targeting YAP or MRTF and treated with increasing doses of BRAFi (Vemurafenib). The sensitivity of M238R cells to BRAFi-induced cell proliferation arrest was partially restored upon YAP or MRTF knockdown, suggesting that collagen stiffening through YAP and MRTF activation contributes to acquired BRAFi resistance (Fig. 2F). Together, these results indicate that the de-differentiated $MITF^{low}/AXL^{high}$ resistant cell state is associated with a mechanophenotype.

$MITF^{low}/AXL^{high}$ BRAFi-resistant cells display YAP and MRTF-dependent contractile activity and assemble an organized ECM. Further functional analysis of the de-differentiated $MITF^{low}$ mesenchymal resistant state revealed that M229R and M238R cells were characterized by high expression levels of typical CAF markers such as caveolin-1 (CAV1), myosin light-chain 2 (MLC2), smooth muscle actin-α (α-SMA), fibroblast activation protein (FAP), transgelin-2 (TAGLN2), in addition to ECM proteins collagen 1 (COL1) and fibronectin (Fig. 3A). In contrast, parental and mutant NRAS-driven resistance M249R cell lines showed low or no expression of such markers. We thus examine whether $MITF^{low}/AXL^{high}$ resistant cells display CAFs-associated features such as ROCK-dependent actomyosin contractility and force-mediated ECM remodeling leading to fibers organization (7,37). We first compared traction stresses generated by sensitive and BRAFi-resistant cells using traction force microscopy (TFM) and observed that M238R cells applied stronger forces on collagen-coated stiff matrices than their drug-sensitive parental counterparts (Fig. 3B). Next, we performed collagen gel contraction assays to assess cell contractility. Contractility in 3D collagen gel was observed for M238R, but not for M238P cells. Inhibition of ROCK by Y27632 or YAP by Verteporfin reduced the capacity of M238R cells to contract collagen gels to levels that are observed for drug-sensitive M238P cells (Fig. 3C). Moreover, siRNA-mediated knockdown of YAP or MRTF abrogated the contractile activity of drug-resistant M238R cells (Fig. 3D).

Given that increased cellular forces lead to matrix fiber organization and that BRAFi-resistant mesenchymal cells secrete high levels of ECM proteins (20,21), we analyzed the topography of the fibronectin and collagen network generated by this resistant cellular state. First, we

compared ECM proteins differentially produced and deposited by M238P and M238R cells. Cell-derived 3D matrices were generated, denuded of cells and analyzed by quantitative mass spectrometry. Compared to M238P cells, M238R cells assembled a matrix that was enriched in ECM glycoproteins (fibronectin, fibrilin-1, thrombospondin-1 and fibulin-1/2), collagens, proteoglycans (versican and biglycan), as well as collagen-modifying enzymes such as transglutaminase 2 and LOXL2 (Supplementary Table S1). Furthermore, in contrast to parental cells, M238R cells produced and assembled fibronectin and collagen fibers oriented in parallel patterns that resembled those produced by TGFβ-activated fibroblasts (Fig. 3E). Fibronectin fibers organization was quantified by measuring the relative orientation angle of fibers. The percentages were 16.5%, 23.7% and 27.8% for M238P, M238R and fibroblasts 3D ECM, respectively (Fig. 3F). Importantly, the lower degree of ECM production by parental cells was not due to a difference in proliferation as evidenced by nuclear and fibronectin stainings of M238P and M238R cell cultures before the decellularization process (Supplementary Fig. S4). Together, these results suggest that $MITF^{low}/AXL^{high}$ BRAFi-resistant cells display increased traction forces and contractility leading to aligned organization of ECM fibers.

Given our observations so far, we explored publicly available expression array studies searching for mechanosignaling, and cell contractility gene expression in drug-resistant human melanoma cell lines. Data extracted from the GEO database (GSE65185) (19) showed increased levels of several YAP/MRTF target genes (*THBS1, CYR61, CTGFAMOTL2, ANKRD1 and SERPINE1)* together with high levels of ECM genes (*COL1A1*, *COL1A2* and *FN1*) and mesenchymal markers (*PDGFRB*, *MYL9*, *ACTA2*, *FAP* and *TAGLN*) in $MITF^{low}/AXL^{high}$ cells developing drug resistance to Vemurafenib (BRAFi) (M229R and SKMel28R) and double resistance to Vemurafenib and Selumetinib (BRAFi + MEKi) (M229DDR and SKMel28DDR) as compared to drug-sensitive parental cell lines (Fig. 3G). Moreover, analysis of gene expression on tumor biopsies from patients progressing during therapy with BRAFi and/or MEKi (GSE50535 and Tirosh *et al* (Supplementary info)) (15,25) revealed that the expression of ECM and mechanosignaling genes markedly increased in a subset of relapsing patients with $MITF^{low}/AXL^{high}$ expression (Fig. 3G).

Early adaptation to MAPK pathway inhibition induces mechanotransduction pathways, contractility and ECM fiber organization. We next questioned whether adaptive response to MAPK pathway inhibition involves mechanosensing pathways and ECM remodeling. *BRAF*-mutant melanoma cells (M238P and 1205Lu) were plated on collagen-coated hydrogels with

medium stiffness and treated with the BRAFi Vemurafenib or the MEKi Trametinib (Fig. 4 and Supplementary Fig. S5). In both cases, drug-treated cells displayed pronounced morphological and actin cytoskeleton changes that were accompanied by increased YAP and MRTF nuclear localization (Fig. 4A and Supplementary Fig. S5A and B), and transcriptional activation of the YAP/MRTF shared target gene *CYR61* relative to untreated cells (Supplementary Fig. S5C). Moreover, drug-treated M238P and 1205Lu cells displayed significantly higher number of FAs with larger size as compared with control cells (Supplementary Fig. S6). We further confirmed that a short-term treatment of cells with either BRAFi or MEKi increased the expression of collagen 1 (COL1) and fibronectin and of the YAP/MRTF target thrombospondin-1 (TSP1), along with reduced phosphorylation of RB and increased expression of p27KIP1, two cell cycle markers that are modulated by MAPK pathway inhibition (Fig. 4B). Importantly, short-term treatment with BRAFi or MEKi was sufficient to increase the contractile activity of 1205Lu cells embedded in 3D collagen gels (Fig. 4C). Consistently, when cultivated one week in the presence of Vemurafenib, 1205Lu cells assembled an organized ECM composed of collagen and fibronectin fibers that were anisotropically oriented, as compared to untreated cells (Fig. 4D). A further indication of the involvement of mechanopathways in the adaptation of melanoma cells to MAPK inhibition was brought by the observation that M238P, 1205Lu and 501Mel cells cultivated on stiff collagen-coated substrates were significantly more resistant to increasing doses of BRAFi as compared to cells cultivated on soft substrates (Fig. 4E). Together, these results demonstrate that melanoma cells rapidly adapt to MAPK pathway inhibition by acquiring an ECM-remodeling contractile phenotype associated with increased mechanosignaling pathways.

Mesenchymal-associated resistance and early adaptation to MAPK pathway inhibition induce the production of a drug-protective ECM. The findings described above support the notion that a subset of BRAF-mutant melanoma cells in response to early and late MAPK pathway inhibition acquire the capacity to produce and remodel a matrix reminiscent to CAF-derived ECM. Because ECM plays a major role in mediating drug resistance, we hypothesized that melanoma cell-derived matrix functions as a supporting niche for melanoma cell behavior. To investigate the effect of melanoma cell-derived ECM on survival and resistance to targeted therapies, drug naïve BRAF-mutant melanoma cells were plated on 3D matrices generated from parental cells (M238P and M229P) or their BRAFi-resistant counterparts (M238R and M229R), and treated or not with Vemurafenib alone or the combination

Vemurafenib/Trametinib (Fig. 5; Supplementary Fig. S7). Time-lapse monitoring of 501Mel proliferation revealed that matrices derived from BRAFi-resistant cells significantly reduced the proliferation arrest induced by MAPK pathway inhibition in contrast to ECMs from BRAFi-sensitive cells, which had no impact on the cytostatic action of BRAF and MEK inhibition (Fig. 5A and B; Supplementary Fig. S7A and B). Cell cycle analysis further confirmed the protective action of matrices from BRAFi-resistant, but not from BRAFi-sensitive cells, over the G0/G1 cell cycle arrest induced by BRAFi on drug-naive 501Mel and MNT1 cells (Fig. 5C; Supplementary Fig. S7C and D). At the molecular level, matrix-mediated therapeutic escape from BRAF inhibition was associated in both 501Mel and MNT1 cells with sustained levels of the proliferation marker phosphorylated-RB and of survivin, low levels of the cell cycle inhibitor p27KIP1 together with maintained phosphorylation of ERK1/2 in presence of the drug (Fig. 5D; Supplementary Fig. S7E and F). Importantly, similar biochemical events were promoted in BRAFi-sensitive 501Mel cells escaping from the combination of BRAFi and MEKi upon adhesion to M238R-derived, but not M238P-derived ECM (Fig. 5E). Next we wondered if short term MAPK pathway inhibition fosters a drug-protective ECM program in melanoma cells. 501Mel cells were plated on matrices generated from vehicle or Vemurafenib-treated 1205Lu cells, and treated with or without BRAFi. Cell cycle and biochemical analysis showed that BRAF inhibition rapidly promoted the production by 1205Lu cells of an ECM that significantly counteracted the cytostatic action of Vemurafenib in 501Mel cells (Fig. 5F and G). Finally, we investigated the involvement of the mechanoresponsive YAP and MRTF transcriptional pathways in ECM-mediated drug protection. 501Mel cells were cultured on matrices prepared from parental M238P or drug-resistant M238R cells and the subcellular location of YAP and MRTF was examined by immunofluorescence microscopy. In contrast to ECM from M238P cells, matrices derived from M238R cells promoted the nuclear translocation of YAP and MRTF (Fig. 6A), and their transcriptional activation as indicated by the increased expression of ANKRD1 and *SERPINE1* genes (Fig. 6B). Consistently, the drug protective action provided by matrices derived from therapy-resistant M238R cells against BRAFi or the combination BRAFi/MEKi was dramatically reduced in 501Mel cells in which either YAP (Fig. 6C) or MRTF (Fig. 6D) expression was knocked-down. Depletion of YAP or MRTF enhanced the efficacy of MAPK pathway inhibition as shown by reduced levels of phosphorylation of ERK1/2 and RB and increased expression of p27KIP1 (Fig. 6E and F). This suggests that melanoma cell-derived ECM mediates drug protection through YAP and MRTF regulation.

Collectively, our findings demonstrate that both early and late adaptation to MAPK pathway inhibition involves the mechanical reprogramming of melanoma cells leading to the assembly of an organized matrix that confers *de novo* resistance to targeted therapies in a YAP and MRTF-dependent manner.

***In vivo* MAPK pathway inhibition promotes melanoma cell-derived ECM accumulation and tumor stiffening.** Exposure of BRAF-mutant melanoma cells to MAPK pathway inhibition promotes a mechanophenotype associated with drug tolerance *in vitro*, which could have important outcomes for disease progression *in vivo*. To address this, we first explored whether BRAF inhibition induces ECM remodeling in human melanoma xenograft models. BRAF-mutant melanoma cells 1205Lu or M229P were xenografted into nude mice (melanoma CDX), which were treated blindly with either vehicle or Vemurafenib (Supplementary Fig. S8A). As expected, BRAF targeting induced a strong inhibition of tumor growth (Supplementary Fig. S8B and C). Histological, transcriptomic and biophysical analyses were then performed at the experiment end point. Vemurafenib treatment triggered a profound remodeling of the 1205Lu (Fig. 7A) and M229P (Supplementary Fig. S8D) tumor stroma, with a marked increase of collagen fibers area and thickness, as measured by polarized light of picrosirius red-labeled tumors and second harmonic generation (SHG) microscopy (Fig. 7A and B; Supplementary Fig. S8D). We then examined gene expression on BRAFi-treated melanoma tumors by performing RT-qPCR analysis using human and mouse probes. Consistent with a previous study (31), Vemurafenib was found to significantly activate tumor-associated host stromal cells. However, compared to untreated tumors, tumors exposed to BRAFi also dramatically upregulated human mesenchymal and ECM genes, including genes for collagens (*COL1A1*, *COL3A1*, *COL5A1*, *COL15A1*), fibronectin (*FN1*), collagen-modifying enzyme (*LOX*) and myofibroblast markers (*SPARC*, *ACTA2*), as well as YAP and/or MRTF target genes, such as *AXL*, *CYR61*, *SERPINE1*, *AMOTL2* and *THBS1* (Fig. 7C). This observation supports the notion that BRAF inhibition can promote a cancer cell-autonomous mechanism of ECM production *in vivo*. Consistent with the changes in ECM composition and assembly, Vemurafenib treatment significantly increased tumor elastic modulus in the two CDX models when measured by atomic force microscopy (AFM) (Fig. 7D; Supplementary Fig. S8E), suggesting that ECM stiffening constitute an adaptive response of melanoma cells to MAPK pathway inhibition *in vivo*. We next wished to validate these observations in melanoma patient-derived xenografts (PDX). PDX exposed or not to the combination of BRAFi and MEKi

were stained with picrosirius red (Fig. 7E). Combined BRAF and MEK inhibition also resulted in a marked accumulation of collagen fibers in the tumor stroma of melanoma PDX (Fig. 7E and F). Finally, Verteporfin, a FDA approved drug used in photodynamic therapy for macular degeneration and a known inhibitor of YAP was used to interrogate if YAP contributes to BRAFi-induced collagen remodeling and therapy response *in vivo*. Whereas Verteporfin alone did not affect 1205Lu melanoma tumor growth, co-treatment with Vemurafenib plus Verteporfin had a greater anti-tumor effect than Vemurafenib alone after 17 days of drug regimens (Fig. 7G and H). Thus, combined Verteporfin and Vemurafenib therapy enhanced Vemurafenib response in a pre-clinical melanoma model. Furthermore, Verteporfin treatment abrogated the accumulation of collagen fibers induced by BRAF inhibition in the stroma of melanoma xenografts (Fig. 7I and J). Together these data suggest that YAP mechanosensing pathway contributes to collagen reorganization in response to MAPK pathway inhibition and support the concept of a combinatorial approach to overcome ECM-mediated therapy resistance in BRAF mutated melanoma models.

DISCUSSION

Pathological ECM remodeling and biomechanical signaling have been linked to tumor aggressiveness in several solid cancers. In the tumor stroma, resident or recruited fibroblasts are activated by tumor-derived factors such as TGFβ to become CAFs, which are considered as the main producers of the tumor ECM (2). In melanoma, BRAFi therapy paradoxically activates melanoma-associated fibroblasts to generate drug-tolerant niches through paracrine HGF or fibronectin secretion (27,31,45). Despite multiple evidence that melanoma cells autonomously produce its own ECM (32,33,46), little is known about the contribution of melanoma cell-derived ECM to drug adaptation and resistance. A major resistance program in BRAF-mutant melanomas exposed to MAPK-targeting therapies is linked to a de-differentiated, mesenchymal transcriptional cell state characterized by low levels of the melanoma differentiation factor MITF and high levels of RTKs including AXL (15,19,21-24). The $MITF^{low}/AXL^{high}$ resistant cells exhibit multiple traits of the Hoek's invasive gene signature (14), including prominent expression of ECM proteins (20,21). Here we showed that this resistant cell population also exhibits key aspects of CAFs involved in ECM remodeling: they acquired a mechanical phenotype associated with an actomyosin/YAP/MRTF-dependent contractile activity, and the ability to deposit ECM to create a tumor-permissive environment. In contrast, drug-naive cells and a population of $MITF^{high}$/NRAS-mutant resistant cells displayed no such mechano-responsive features and ECM remodeling activities. Importantly, we also found that early adaptation to MAPK pathway inhibition promotes *de novo* acquisition of a CAF-like phenotype leading to biomechanical reprogramming both *in vitro* and *in vivo*. We thus uncover a previously unidentified feed-forward loop between drug-exposed or resistant $MITF^{low}/AXL^{high}$ melanoma cells and ECM remodeling to increase tumor tissue stiffness, mechanosensing and resistance through YAP and MRTF regulation (Fig. 7K).

We showed that short-term treatment of melanoma cells with targeted drugs induced actin dynamics, mechanosensitive regulation of YAP and MRTF and increased melanoma cell contractility. This differs from another early adaptation state to BRAF inhibition characterized by the emergence of a slow-cycling $NGFR/CD271^{high}$ persistent cell population (20). However, our results are in line with the observation that BRAFi modulates actin reorganization and YAP/TAZ activation (11) as well as Rho GTPase signaling (47). Thus, our findings underscore the exquisite phenotypic plasticity of melanoma cells and the notion that their biomechanical reprogramming may actively participate to tumor heterogeneity and therapeutic escape.

Another indication of the ability of targeted therapies to switch melanoma cells towards a CAF-like phenotype is based on our findings that BRAFi induces melanoma cells to autonomously remodel a fibrillar and drug-protective ECM network, an additional trait typical of CAFs. A previous study has shown that short-term BRAF inhibition up-regulates adhesion signaling and drug tolerance in *BRAF*-mutant/*PTEN*-null melanoma cells (48). Extending this observation, our data demonstrate that short-term MAPK pathway inhibition induces the assembly by melanoma cells of an aligned ECM containing collagens, fibronectin and thrombospondin-1, indicating that targeted therapies have the capacity to rapidly exacerbate the intrinsic ability of melanoma cells to produce a pro-invasive ECM (32,46). Vemurafenib treatment was shown to activate melanoma-associated fibroblasts to generate a drug-tolerant niche through fibronectin-mediated integrin β1/FAK signaling (31). In this study, cell death following BRAF inhibition was reduced when melanoma cells were cultured on stiff substrates containing the combination of fibronectin, thrombospondin-1 and tenascin-C (31). A part from ECMs assembled by therapy-activated fibroblasts, our study reveals a crucial role of fibronectin and collagen-rich ECMs derived from either drug-resistant or drug-exposed melanoma cells in driving tolerance. The protection against the cytostatic effect of MAPK inhibition brought by melanoma-derived matrices is evidenced by the persistence of cycling cells, with sustained levels of proliferative markers and YAP/MRTF nuclear translocation. Remarkably, tolerance to BRAFi was achieved when BRAF-mutant melanoma cells were plated on collagen-coated stiff matrices, supporting the notion that, in addition to fibronectin (31,48), the collagen network and ECM stiffening are major mediators of melanoma drug resistance. Interestingly, previous studies with bioengineered materials have shown the impact of substrate stiffness on targeted drugs responses in melanoma (49) and carcinoma cell lines (50).

YAP-TEAD and MRTF-SRF pathways functionally interact to coordinate mechanosignaling required for the maintenance of the CAF phenotype in solid tumors (7-9,51). Similarly, we showed that the contractile behavior of the de-differentiated resistant melanoma cells requires YAP and MRTF expression. Importantly, we found that YAP and MRTF are activated upon mechanical stress and contribute to ECM-mediated drug resistance. This is in agreement with recent reports demonstrating the contribution of the YAP pathway in BRAFi resistance (10-12). However, these studies were conducted on rigid plastic dishes that do not reflect tissue mechanical compliance. In contrast, we demonstrated the exacerbated ability of de-differentiated resistant and BRAFi-exposed melanoma cells to adapt to substrate rigidity

using cell-derived 3D ECMs and collagen-coated hydrogels with defined stiffness, which model more accurately the activation of YAP and MRTF mechanosensors. In contrast to YAP-TEAD pathway, the role of MRTF-SRF pathway in melanoma therapeutic resistance remains less defined. MRTF controls several cytoskeletal genes, including α-SMA and MLC2 (8) that we found enriched in the $MITF^{low}/AXL^{high}$ resistant cells and in $MITF^{low}$ tumor biopsies from progressing melanoma patients. Moreover, several components of the matrisome from $MITF^{low}$ resistant cells, such as tenascin-C, CYR61, thrombospondin-1 and serpine1 are known YAP and/or MRTF targets (9). Remarkably, a YAP1 enrichment signature has also been identified as a driver event of melanoma acquired resistance (19). This is in line with our *in silico* gene expression analyses from public datasets that revealed a similar trend towards an increased expression of YAP/MRTF target genes in $MITF^{low}$ tumor biopsies from patients relapsing from therapy. Of note, a recent study identified AXL, a RTK required to maintain the resistant phenotype in melanoma (24), in a YAP/TAZ target gene signature (52). Accordingly, we found several YAP/MRTF target genes including AXL induced upon BRAFi treatment in our xenograft model. This raises the possibility that the reservoir of AXL^{high} resistant cells is promoted by biomechanical adaptation of melanoma cells to oncogenic BRAF pathway inhibition. Interestingly, collagen stiffening has been recently shown to promote melanoma differentiation via YAP/PAX3-mediated MITF expression (53). This study and our present report support the emerging notion that collagen density and rigidity is a key microenvironmental factor that governs melanoma cell plasticity and intra-tumor heterogeneity. How YAP and MRTF actually coordinate mechanical signals from tumor microenvironments to drive melanoma differentiation, invasive behavior or drug resistance is currently unknown and requires further investigations.

Importantly, our data reveal a targetable vulnerability of Vemurafenib-induced mechanical reprograming of melanoma *in vivo*. Melanoma tumors treated with BRAFi or combined BRAFi/MEKi therapy displayed an intense remodeling of the tumor niche associated to increased collagen fibers organization and YAP/MRTF-mediated gene expression. Earlier studies have underscored the critical role of melanoma-associated fibroblasts activated by BRAF inhibition for the development of resistant niches (27,28,31,45). Accordingly, we found that host stromal cells that likely include fibroblasts produce some ECM genes in response to Vemurafenib. However, we demonstrated that the molecular changes associated with the dramatic remodeling of the tumor niche in response to MAPK pathway inhibition also results from the activation of human melanoma cells, thereby promoting an autocrine production of a

rigid ECM enriched in collagen fibers. In line with the key role of the YAP pathway during melanoma relapse (19) and phenotypic heterogeneity (12), we found that YAP-TEAD inhibition by Verteporfin reverses Vemurafenib-induced excessive collagen deposition. Consequently, melanoma tumors treatment with Verteporfin cooperated with Vemurafenib to reduce tumor growth. Whether targeting MRTF-SRF signaling pathway may also demonstrate therapeutic efficiency is currently under investigation.

In conclusion, our findings disclose a novel mechanism of BRAF-mutant melanoma cells adaptation to MAPK-targeted therapies through the acquisition of an auto-amplifying CAF-like phenotype in which melanoma cell-derived ECM modulates mechanosensing pathways to promote tumor stiffening. In addition to therapy-induced tumor secretomes (54), therapy-induced mechanical phenotypes could endow cancer cells with unique cell-autonomous abilities to survive and differentiate within challenging tumor-associated microenvironments, thereby contributing to drug resistance and relapse. Our results suggest that cancer cell-ECM interactions and tumor mechanics provide promising targets for therapeutic intervention aimed at enhancing targeted therapies efficacy in melanoma.

Acknowledgments. We thank R.S. Lo for M229P/R, M238P/R and M249P/R melanoma cells. We acknowledge the C3M animal room facility and the C3M imaging facility. The SHG microscopy was done at MICA facility, in the IBV-CNRS UMR 7277-INSERM U1091-UNS. We thank TRACE (PDX platform at the KULeuven University) for providing the PDX models.

Author contributions. M.D. and S.T.D. supervised and designed the study. C.A.G. designed the experiments. C.A.G., M.L and R.B.J. performed the experiments and analyzed the data with the help of I.B., S.D., V.P. and A.M. F.L. performed flow cytometry analyses. M.G. provided technical advice and expertise in microscopy. S.P. performed AFM analyses. S.S. performed SGH microscopy analyses. S.A. performed mass spectrometry analyses. B.M. and C.G. contributed reagents and expertise. E.L and J.C.M. contributed to PDX studies. M.D. and S.T.D. wrote the manuscript with the help of C.A.G. and input from all the others authors.

REFERENCES

1. Lu P, Weaver VM, Werb Z. The extracellular matrix: a dynamic niche in cancer progression. J Cell Biol **2012**;196:395-406
2. Levental KR, Yu H, Kass L, Lakins JN, Egeblad M, Erler JT*, et al.* Matrix crosslinking forces tumor progression by enhancing integrin signaling. Cell **2009**;139:891-906
3. Laklai H, Miroshnikova YA, Pickup MW, Collisson EA, Kim GE, Barrett AS*, et al.* Genotype tunes pancreatic ductal adenocarcinoma tissue tension to induce matricellular fibrosis and tumor progression. Nat Med **2016**;22:497-505
4. Hinz B. The myofibroblast: paradigm for a mechanically active cell. J Biomech **2010**;43:146-55
5. Paszek MJ, Zahir N, Johnson KR, Lakins JN, Rozenberg GI, Gefen A*, et al.* Tensional homeostasis and the malignant phenotype. Cancer Cell **2005**;8:241-54
6. Dupont S, Morsut L, Aragona M, Enzo E, Giulitti S, Cordenonsi M*, et al.* Role of YAP/TAZ in mechanotransduction. Nature **2011**;474:179-83
7. Calvo F, Ege N, Grande-Garcia A, Hooper S, Jenkins RP, Chaudhry SI*, et al.* Mechanotransduction and YAP-dependent matrix remodelling is required for the generation and maintenance of cancer-associated fibroblasts. Nat Cell Biol **2013**;15:637-46
8. Finch-Edmondson M, Sudol M. Framework to function: mechanosensitive regulators of gene transcription. Cell Mol Biol Lett **2016**;21:28
9. Foster CT, Gualdrini F, Treisman R. Mutual dependence of the MRTF-SRF and YAP-TEAD pathways in cancer-associated fibroblasts is indirect and mediated by cytoskeletal dynamics. Genes Dev **2017**;31:2361-75
10. Lin L, Sabnis AJ, Chan E, Olivas V, Cade L, Pazarentzos E*, et al.* The Hippo effector YAP promotes resistance to RAF- and MEK-targeted cancer therapies. Nat Genet **2015**;47:250-6
11. Kim MH, Kim J, Hong H, Lee SH, Lee JK, Jung E*, et al.* Actin remodeling confers BRAF inhibitor resistance to melanoma cells through YAP/TAZ activation. EMBO J **2016**;35:462-78
12. Verfaillie A, Imrichova H, Atak ZK, Dewaele M, Rambow F, Hulselmans G*, et al.* Decoding the regulatory landscape of melanoma reveals TEADS as regulators of the invasive cell state. Nat Commun **2015**;6:6683
13. Shain AH, Bastian BC. From melanocytes to melanomas. Nat Rev Cancer **2016**;16:345-58
14. Widmer DS, Cheng PF, Eichhoff OM, Belloni BC, Zipser MC, Schlegel NC*, et al.* Systematic classification of melanoma cells by phenotype-specific gene expression mapping. Pigment Cell Melanoma Res **2012**;25:343-53
15. Tirosh I, Izar B, Prakadan SM, Wadsworth MH, 2nd, Treacy D, Trombetta JJ*, et al.* Dissecting the multicellular ecosystem of metastatic melanoma by single-cell RNA-seq. Science **2016**;352:189-96
16. Tsoi J, Robert L, Paraiso K, Galvan C, Sheu KM, Lay J*, et al.* Multi-stage Differentiation Defines Melanoma Subtypes with Differential Vulnerability to Drug-Induced Iron-Dependent Oxidative Stress. Cancer Cell **2018**;33:890-904 e5
17. Flaherty KT, Hodi FS, Fisher DE. From genes to drugs: targeted strategies for melanoma. Nat Rev Cancer **2012**;12:349-61

18. Shi H, Hugo W, Kong X, Hong A, Koya RC, Moriceau G, *et al.* Acquired resistance and clonal evolution in melanoma during BRAF inhibitor therapy. Cancer Discov **2014**;4:80-93
19. Hugo W, Shi H, Sun L, Piva M, Song C, Kong X, *et al.* Non-genomic and Immune Evolution of Melanoma Acquiring MAPKi Resistance. Cell **2015**;162:1271-85
20. Titz B, Lomova A, Le A, Hugo W, Kong X, Ten Hoeve J, *et al.* JUN dependency in distinct early and late BRAF inhibition adaptation states of melanoma. Cell Discov **2016**;2:16028
21. Nazarian R, Shi H, Wang Q, Kong X, Koya RC, Lee H, *et al.* Melanomas acquire resistance to B-RAF(V600E) inhibition by RTK or N-RAS upregulation. Nature **2010**;468:973-7
22. Villanueva J, Vultur A, Lee JT, Somasundaram R, Fukunaga-Kalabis M, Cipolla AK, *et al.* Acquired resistance to BRAF inhibitors mediated by a RAF kinase switch in melanoma can be overcome by cotargeting MEK and IGF-1R/PI3K. Cancer Cell **2010**;18:683-95
23. Girotti MR, Pedersen M, Sanchez-Laorden B, Viros A, Turajlic S, Niculescu-Duvaz D, *et al.* Inhibiting EGF receptor or SRC family kinase signaling overcomes BRAF inhibitor resistance in melanoma. Cancer Discov **2013**;3:158-67
24. Muller J, Krijgsman O, Tsoi J, Robert L, Hugo W, Song C, *et al.* Low MITF/AXL ratio predicts early resistance to multiple targeted drugs in melanoma. Nat Commun **2014**;5:5712
25. Sun C, Wang L, Huang S, Heynen GJ, Prahallad A, Robert C, *et al.* Reversible and adaptive resistance to BRAF(V600E) inhibition in melanoma. Nature **2014**;508:118-22
26. Rathore M, Girard C, Ohanna M, Tichet M, Ben Jouira R, Garcia E, *et al.* Cancer cell-derived long pentraxin 3 (PTX3) promotes melanoma migration through a toll-like receptor 4 (TLR4)/NF-kappaB signaling pathway. Oncogene **2019**;38:5873-89
27. Straussman R, Morikawa T, Shee K, Barzily-Rokni M, Qian ZR, Du J, *et al.* Tumour micro-environment elicits innate resistance to RAF inhibitors through HGF secretion. Nature **2012**;487:500-4
28. Kaur A, Webster MR, Marchbank K, Behera R, Ndoye A, Kugel CH, 3rd, *et al.* sFRP2 in the aged microenvironment drives melanoma metastasis and therapy resistance. Nature **2016**;532:250-4
29. Smith MP, Sanchez-Laorden B, O'Brien K, Brunton H, Ferguson J, Young H, *et al.* The immune microenvironment confers resistance to MAPK pathway inhibitors through macrophage-derived TNFalpha. Cancer Discov **2014**;4:1214-29
30. Young HL, Rowling EJ, Bugatti M, Giurisato E, Luheshi N, Arozarena I, *et al.* An adaptive signaling network in melanoma inflammatory niches confers tolerance to MAPK signaling inhibition. J Exp Med **2017**;214:1691-710
31. Hirata E, Girotti MR, Viros A, Hooper S, Spencer-Dene B, Matsuda M, *et al.* Intravital imaging reveals how BRAF inhibition generates drug-tolerant microenvironments with high integrin beta1/FAK signaling. Cancer Cell **2015**;27:574-88
32. Gaggioli C, Robert G, Bertolotto C, Bailet O, Abbe P, Spadafora A, *et al.* Tumor-derived fibronectin is involved in melanoma cell invasion and regulated by V600E B-Raf signaling pathway. J Invest Dermatol **2007**;127:400-10

33. Naba A, Clauser KR, Hoersch S, Liu H, Carr SA, Hynes RO. The matrisome: in silico definition and in vivo characterization by proteomics of normal and tumor extracellular matrices. Mol Cell Proteomics **2012**;11:M111 014647
34. Didier R, Mallavialle A, Ben Jouira R, Domdom MA, Tichet M, Auberger P*, et al.* Targeting the Proteasome-Associated Deubiquitinating Enzyme USP14 Impairs Melanoma Cell Survival and Overcomes Resistance to MAPK-Targeting Therapies. Mol Cancer Ther **2018**;17:1416-29
35. Tichet M, Prod'Homme V, Fenouille N, Ambrosetti D, Mallavialle A, Cerezo M*, et al.* Tumour-derived SPARC drives vascular permeability and extravasation through endothelial VCAM1 signalling to promote metastasis. Nat Commun **2015**;6:6993
36. Beacham DA, Amatangelo MD, Cukierman E. Preparation of extracellular matrices produced by cultured and primary fibroblasts. Curr Protoc Cell Biol **2007**;Chapter 10:Unit 10 9
37. Albrengues J, Bourget I, Pons C, Butet V, Hofman P, Tartare-Deckert S*, et al.* LIF mediates proinvasive activation of stromal fibroblasts in cancer. Cell Rep **2014**;7:1664-78
38. Martiel JL, Leal A, Kurzawa L, Balland M, Wang I, Vignaud T*, et al.* Measurement of cell traction forces with ImageJ. Methods Cell Biol **2015**;125:269-87
39. Tse JR, Engler AJ. Preparation of hydrogel substrates with tunable mechanical properties. Curr Protoc Cell Biol **2010**;Chapter 10:Unit 10 6
40. Estrach S, Lee SA, Boulter E, Pisano S, Errante A, Tissot FS*, et al.* CD98hc (SLC3A2) loss protects against ras-driven tumorigenesis by modulating integrin-mediated mechanotransduction. Cancer Res **2014**;74:6878-89
41. Rambow F, Rogiers A, Marin-Bejar O, Aibar S, Femel J, Dewaele M*, et al.* Toward Minimal Residual Disease-Directed Therapy in Melanoma. Cell **2018**;174:843-55 e19
42. Bertero T, Oldham WM, Cottrill KA, Pisano S, Vanderpool RR, Yu Q*, et al.* Vascular stiffness mechanoactivates YAP/TAZ-dependent glutaminolysis to drive pulmonary hypertension. J Clin Invest **2016**;126:3313-35
43. Humphrey JD, Dufresne ER, Schwartz MA. Mechanotransduction and extracellular matrix homeostasis. Nat Rev Mol Cell Biol **2014**;15:802-12
44. Zhao XH, Laschinger C, Arora P, Szaszi K, Kapus A, McCulloch CA. Force activates smooth muscle alpha-actin promoter activity through the Rho signaling pathway. J Cell Sci **2007**;120:1801-9
45. Fedorenko IV, Wargo JA, Flaherty KT, Messina JL, Smalley KSM. BRAF Inhibition Generates a Host-Tumor Niche that Mediates Therapeutic Escape. J Invest Dermatol **2015**;135:3115-24
46. Chapman A, Fernandez del Ama L, Ferguson J, Kamarashev J, Wellbrock C, Hurlstone A. Heterogeneous tumor subpopulations cooperate to drive invasion. Cell Rep **2014**;8:688-95
47. Klein RM, Spofford LS, Abel EV, Ortiz A, Aplin AE. B-RAF regulation of Rnd3 participates in actin cytoskeletal and focal adhesion organization. Mol Biol Cell **2008**;19:498-508
48. Fedorenko IV, Abel EV, Koomen JM, Fang B, Wood ER, Chen YA*, et al.* Fibronectin induction abrogates the BRAF inhibitor response of BRAF V600E/PTEN-null melanoma cells. Oncogene **2016**;35:1225-35

49. Tokuda EY, Leight JL, Anseth KS. Modulation of matrix elasticity with PEG hydrogels to study melanoma drug responsiveness. Biomaterials **2014**;35:4310-8
50. Nguyen TV, Sleiman M, Moriarty T, Herrick WG, Peyton SR. Sorafenib resistance and JNK signaling in carcinoma during extracellular matrix stiffening. Biomaterials **2014**;35:5749-59
51. Cordenonsi M, Zanconato F, Azzolin L, Forcato M, Rosato A, Frasson C*, et al.* The Hippo transducer TAZ confers cancer stem cell-related traits on breast cancer cells. Cell **2011**;147:759-72
52. Wang Y, Xu X, Maglic D, Dill MT, Mojumdar K, Ng PK*, et al.* Comprehensive Molecular Characterization of the Hippo Signaling Pathway in Cancer. Cell Rep **2018**;25:1304-17 e5
53. Miskolczi Z, Smith MP, Rowling EJ, Ferguson J, Barriuso J, Wellbrock C. Collagen abundance controls melanoma phenotypes through lineage-specific microenvironment sensing. Oncogene **2018**;37:3166-82
54. Obenauf AC, Zou Y, Ji AL, Vanharanta S, Shu W, Shi H*, et al.* Therapy-induced tumour secretomes promote resistance and tumour progression. Nature **2015**;520:368-72

FIGURES LEGENDS

Figure 1: Mesenchymal BRAFi-resistant melanoma cells display increased mechanosensitivity and proliferation on collagen stiff substrate. (A) Representative images of parental (M238P) versus mesenchymal BRAFi-resistant (M238R) cell morphology after 48 h culture on collagen-coated hydrogels of increasing stiffness (low: 0.2 kPa; medium: 4 kPa; high: 50 kPa). Fluorescence stains represent F-actin (green) and nucleus (blue). Scale bar, 100 µm. Insets show higher magnification views. **(B)** Quantification of cell morphological changes (area, roundness). Data is represented as scatter plot with mean ± s.d. from 10 samples. ***P*<0.01, ****P*<0.001, Kruskall-Wallis analysis. **(C)** Morphology of mesenchymal BRAFi-resistant M229R and of BRAFi-resistant M249R harboring a secondary NRAS mutation cells compared to parental cells, 48 h after plating on hydrogels of intermediate stiffness (4 kPa). Fluorescence stains represent F-actin (green) and nucleus (blue). Scale bar, 100 µm. Insets show higher magnification views. **(D)** Quantification of morphological changes (area, roundness) of M229R, M249R and their parental lines (M229P, M249P) on hydrogels of medium stiffness. Data is represented as scatter plot with mean ± s.d from 10 samples. **P*<0.05, ***P*<0.01, ****P*<0.001, Kruskall-Wallis analysis. **(E)** Bar plot of cell number quantification of parental and resistant melanoma cells cultured for 72 h on collagen low (0.2 kPa) versus high (50 kPa) stiffness. Cells were counted by Hoechst-labeled nuclei staining. Data are normalized to the parental cells on soft substrate. **P*<0.05, ***P*<0.01, ****P*<0.001, 2-way ANOVA analysis.

Figure 2: The mechanosensors YAP and MRTF are activated in mesenchymal BRAFi-resistant melanoma cells. Effect of substrate stiffening on YAP **(A)** and MRTF **(B)** nuclear translocation assessed by immunofluorescence in M238P versus M238R cells cultured for 48 h on collagen-coated hydrogels of increasing stiffness. *Left panels*, representative images. Insets show nuclei staining by DAPI on the same fields. Scale bar, 40 µm. *Right panels*, bar graphs show the proportion of single cells in which YAP and MRTF were located either in the nucleus (N) or in the cytoplasm (C), as a function of stiffness (n = 3; 30 cells/condition per experiment). **(C)** qPCR analysis of the expression of YAP-MRTF target genes in M238P and M238R cells plated for 48 h on substrates with increased stiffness (low: 0.2 kPa; medium: 4 kPa; high: 50 kPa). Data are normalized to the expression in parental cells plated on soft (L) substrate. Data is represented as mean ± s.d. from 3 samples. **P*<0.05, ***P*<0.01, ****P*<0.001,

2-way ANOVA analysis. **(D)** M238R cells plated on high stiffness substrate were treated with 10 μM of Y27632 for 48 h. Nuclear versus cytoplasmic location of YAP and MRTF was assessed by immunofluorescence. *Upper panel,* data are represented as scatter plots with mean ± s.d. from >30 cells. ***P<0.001, Kruskall-Wallis analysis. *Lower panel,* representative immunofluorescence images of YAP (left) and MRTF (right). Scale bar, 20 μm. **(E)** qPCR analysis of *CYR61* and *CTGF* expression in M238R cells plated on high stiffness substrate and treated with 10 μM of Y27632 for 72 h. Data are normalized to the expression in vehicle treated cells. Data are the mean ± s.d. from 3 samples. ***P<0.001, 2-way ANOVA analysis. **(F)** Vemurafenib dose response curves from MTS proliferation assays of M238R cells transfected with control siRNA (siCtrl), siYAP or siMRTF. *Right panel,* protein lysates from transfected cells were immunoblotted for YAP and MRTF expression. HSP90, loading control.

Figure 3: Mesenchymal BRAFi-resistant melanoma cells produce an organized ECM fibrillar network through increased contraction forces and contractility. (A) Immunoblot analysis of myofibroblast markers on lysates from BRAFi-resistant cells compared to parental cells. HSP90, loading control. **(B)** Heat scale plot showing the traction forces applied by M238P versus M238R seeded on 4kPa fluorescent bead-embedded collagen-coated hydrogels for 48 h. *Bottom panel,* quantification of contractile forces applied by the cells. Data is the mean ± s.d. (n=30 fluorescent bead displacement measured per cell from 6 cells). ***P<0.001, Kruskall-Wallis analysis. **(C)** Collagen gel contraction assays of M238P and M238R cells in presence or not of Y27632 (10 μM) or Verteporfin (1 μM). Representative images of contraction assays are shown. *Bottom panel,* quantification of gel contraction (percent). Bar graph represents the mean ± s.d. of triplicate experiments. ***P<0.001, Kruskall-Wallis test. **(D)** Collagen gel contraction assays of M238R transfected with a siRNA Control (siCtrl), siYAP or siMRTF. Representative images of contraction assays are shown. *Bottom panel,* quantification of the percentage of gel contraction. Bar graph is mean ± s.d. of triplicate experiments. **P<0.01, ***P<0.001. **(E)** Fibronectin and collagen staining of decellularized 3D ECM derived from M238P cells, M238R cells or skin fibroblasts. *Top panels*, anti-fibronectin immunofluorescence; *Bottom panels*, picrosirius red staining. Scale bar, 50 μm. **(F)** Quantification of fibronectin fibers orientation in ECMs from parental and BRAFi-resistant cells. Fibronectin fibers were visualized as in (D) and their orientation angles plotted as a frequency distribution. Percentages indicate oriented fibers accumulated in a range of ± 21° around the modal angle. Data is represented as mean ± s.d. (n=10 random fields from a

duplicate determination). ***P<0.001, Kruskall-Wallis analysis. **(G)** Heatmap showing the differential expression of selected genes in melanoma cell lines or patient (Pt) biopsies upon BRAFi and/or MEKi treatment. Data were extracted from public datasets of human melanoma cell line developing resistance to BRAFi and double resistance to BRAFi/MEKi compared to drug-naive cell lines (GSE65185) and from datasets of melanoma biopsies from patients before and after development of resistance to BRAFi (*), MEKi (°) or BRAFi/MEKi combination (*°) (GSE50535; Tirosh *et al.* Supplementary information).

Figure 4: MAPK signaling inhibition triggers mechanoactivation pathways, melanoma cell contractility activity and ECM fibril alignment. (A) Representative images of YAP and MRTF immunostaining of drug-sensitive 1205Lu cells plated for 48 h on 2.8kPa collagen-coated hydrogels and treated with 1% DMSO (vehicle), 3 µM Vemurafenib (BRAFi) or 1 µM Trametinib (MEKi). Scale bar, 40 µm. Insets show nuclei staining by DAPI on the same images. *Bottom panels*, quantification of the nucleocytoplasmic distribution of YAP (*left*) and MRTF (*right*) (n = 3; 30 cells/condition per experiment). **(B)** Collagen gel contraction assays of 1205Lu cells pre-treated for 72 h with 1% DMSO (vehicle), 3 µM Vemurafenib (BRAFi) or 1 µM Trametinib (MEKi). *Right panel,* quantification of the percentage of gel contraction. Bar graph is the mean ± s.d. of triplicate experiments. ***P<0.001**. (C)** Immunoblot analysis of ECM proteins and cell proliferation markers on lysates from M238P and 1205Lu cells treated as above. Tubulin, loading control. **(D)** Immunofluorescence analysis of fibronectin and collagen I fibers assembly in decellularized ECM generated from 1205Lu cells treated with vehicle (DMSO) or Vemurafenib for 7 days. Scale bar, 40 µm. *Left histograms,* quantification of fibronectin fibers orientation. Percentages indicate fibers accumulated in a range of ± 21° around the modal angle. **(E)** Indicated melanoma cells were cultured on low (0.2 kPa) *versus* high (50 kPa) stiffness substrate for 72 h in the presence of the indicated dose of Vemurafenib. Bar graphs show cell number quantification by Incucyte analysis of NucLight red-labeled cell nuclei. Data are normalized relative to the number of cells on soft substrate and 1µM Vemurafenib. *P<0.05, **P<0.01, ***P<0.001, 2-way ANOVA analysis.

Figure 5: Early adaptation and mesenchymal-associated resistance to MAPK pathway inhibition is associated with the production of a drug-protective ECM. (A) Proliferation curves of 501Mel cells cultured on decellularized 3D cell-derived matrices generated from parental (M238P) or BRAFi-resistant (M238R) melanoma cells and treated with vehicle or

with 2 μM Vemurafenib in combination or not with 0.1 μM Trametinib. Time-lapse analysis of fluorescently NucLight™-labeled 501Mel cells using the IncuCyte system. Graphs show quantification of cell numbers from NucLight Red nuclear object counting. Data are the mean ± s.d. (n=3). ***P<0.001, 2-way ANOVA analysis. A.U. arbitrary unit. **(B)** Representative images of nuclear labeling and red fluorescence at the end of the experiment shown in A (120 h). **(C)** Cell cycle distribution of 501Mel (*top graph*) or MNT1 (*bottom graph*) cells cultured on M238P or M238R cell-derived ECM for 48 h and treated for an additional 48 h with vehicle (DMSO) or 2 μM Vemurafenib. Histograms represent the percentage of cells in different phases of the cell cycle. **(D)** Immunoblot analysis of cell cycle markers on lysates from 501Mel and MNT1 cells from experiments shown in C. **(E)** Immunoblot analysis of cell cycle markers on lysates from 501Mel cells cultured on M238P or M238R cell-derived ECM treated for 48 h with a combination of 2 μM Vemurafenib and 0.1 μM Trametinib. **(F)** Cell cycle distribution of 501Mel cells cultured on cell-derived matrices generated from vehicle or Vemurafenib-treated 1205lu cells and treated with vehicle (DMSO) or 2 μM Vemurafenib for 48 h. Cell cycle profiles were analyzed as above. **(G)** Immunoblot analysis of cell cycle markers on lysates from 501Mel cells obtained from F.

Figure 6: Matrices generated by resistant melanoma cells induces YAP and MRTF activation to confer protection to MAPK pathway inhibition. (A) 501Mel cells were cultured on M238P or M238R cell-derived matrices for 48 h and subjected to immunofluorescence analysis of YAP (red) and MRTF (green). Insets show nuclei staining by DAPI on the same fields. Scale bar, 40 μm. *Right panel,* quantification of the nucleocytoplasmic distribution of YAP and MRTF (n>30 cells, ***P<0.001). P-values were determined using Mann-Whitney U test. **(B)** RT-qPCR analysis of shared YAP/MRTF target genes expression in 501Mel cells obtained from A. Data is represented as mean ± s.d. from 3 samples. *P<0.05, **P<0.01, 2-way ANOVA analysis. **(C, D)** Bar graphs showing the quantification of cell proliferation of 501Mel plated on M238P or M238R cell-derived matrices and treated for 72 h with vehicle or with 2 μM Vemurafenib in combination or not with 0.1 μM Trametinib following transfection with control siRNA (siCtrl) or YAP (siYAP) siRNA (C), or following transfection with siCtrl or MRTF (siMRTF) siRNA (D). Data are the mean ± s.d. (n=3). *$P<0.05$, ***P<0.001 (2 way-ANOVA). *Right panels* in C and D show immunoblots of YAP and MRTF levels in transfected cells. HSP60, loading control. **(E, F)** Immunoblot analysis of cell cycle

markers on lysates obtained from the experiments described in (C) and (D). ERK2, loading control.

Figure 7: *In vivo* MAPK inhibition drives melanoma cell biomechanical reprogramming and tumor stiffening in human melanoma tumors. (A) Sections of 1205Lu melanoma cell-derived xenografts (CDX) treated with DMSO (vehicle) or with Vemurafenib (BRAFi) were stained with picrosirius red and imaged under original bright field (parallel, *top*) or polarized light (orthogonal, bottom). Scale bar, 500 µM. Collagen fibers area was quantified from picrosirius red stainings with Image J software. Values represent mean ± s.d. of 4 independent fields. **P*<0.05, ***P*<0.01. **(B)** Second harmonic generation (SHG)microscopy from samples described in (A). Scale bar, 500 µM. SHG intensity was quantified with Image J software. Values represent mean ± s.d. of 4 independent fields. **P*<0.05, ***P*<0.01. **(C)** Heatmap showing the differential expression of a selection of human and mouse ECM genes, dedifferentiation markers and YAP/MRTF target genes in untreated *versus* Vemurafenib-treated 1205Lu melanoma tumors. Gene expression was assessed by RT-qPCR. **(D)** Scatter plot with mean ± s.d. showing Young's modulus (E_{app}) measurements of vehicle and Vemurafenib-treated 1205Lu tumors. *****P*<0.0001. **(E)** Tumor sections obtained from melanoma patient-derived xenografts (PDX) that were treated or not with BRAFi (Dabrafenib) and MEKi (Trametinib) were stained with hematoxylin/eosin or picrosirius red, and imaged under transmission (parallel) or polarized light (orthogonal) microscopy. Scale bar, 150 µM. **(F)** Collagen fibers area was quantified from picrosirius red stainings with Image J software. Values represent mean ± s.d. of 4 independent fields. **(G)** 1205Lu cells (1×10^6) were injected s.c. into nude mice. Tumor volume was assessed with caliper and when tumors reached 100 mm^3, mice were randomized into four groups and were administered (i.p. injection) vehicle (DMSO), Vemurafenib (BRAFi) (35 mg/kg), Verteporfin (a YAP/TEAD inhibitor) (45 mg/kg), or the combination of Vemurafenib and Verteporfin for 19 days. Data shown are mean ± s.d. *Left panels*, photographs of representative mice and tumors taken at day 19 are shown. **(H)** Bar graphs showing tumor weights at the end of the experiments shown in G. Data are means ± s.d. (*n*=6; **P*<0.05, ***P*<0.01, ****P*<0.01, Kruskall-Wallis test). **(I)** Sections of 1205Lu melanoma CDX tumors from the experiment shown in G were stained with hematoxylin/eosin or picrosirius red, and imaged under transmission (parallel) or polarized light (orthogonal) microscopy. **(J)** Bar graphs showing the quantification of collagen fibers area on images of tumor sections obtained from I. Values are the mean ± s.d. of 4 independent fields. ***P*<0.01,

***P<0.001, Kruskall-Wallis test. **(K)** Proposed model for the biomechanical reprogramming of melanoma cell induced by MAPK targeted therapies. The scheme shows the reciprocal YAP/MRTF-dependent feed-forward loop between drug-exposed or resistant $MITF^{low}/AXL^{high}$ melanoma cells and ECM remodeling to increase tumor tissue stiffening, mechanosensing and resistance.

Figure 1

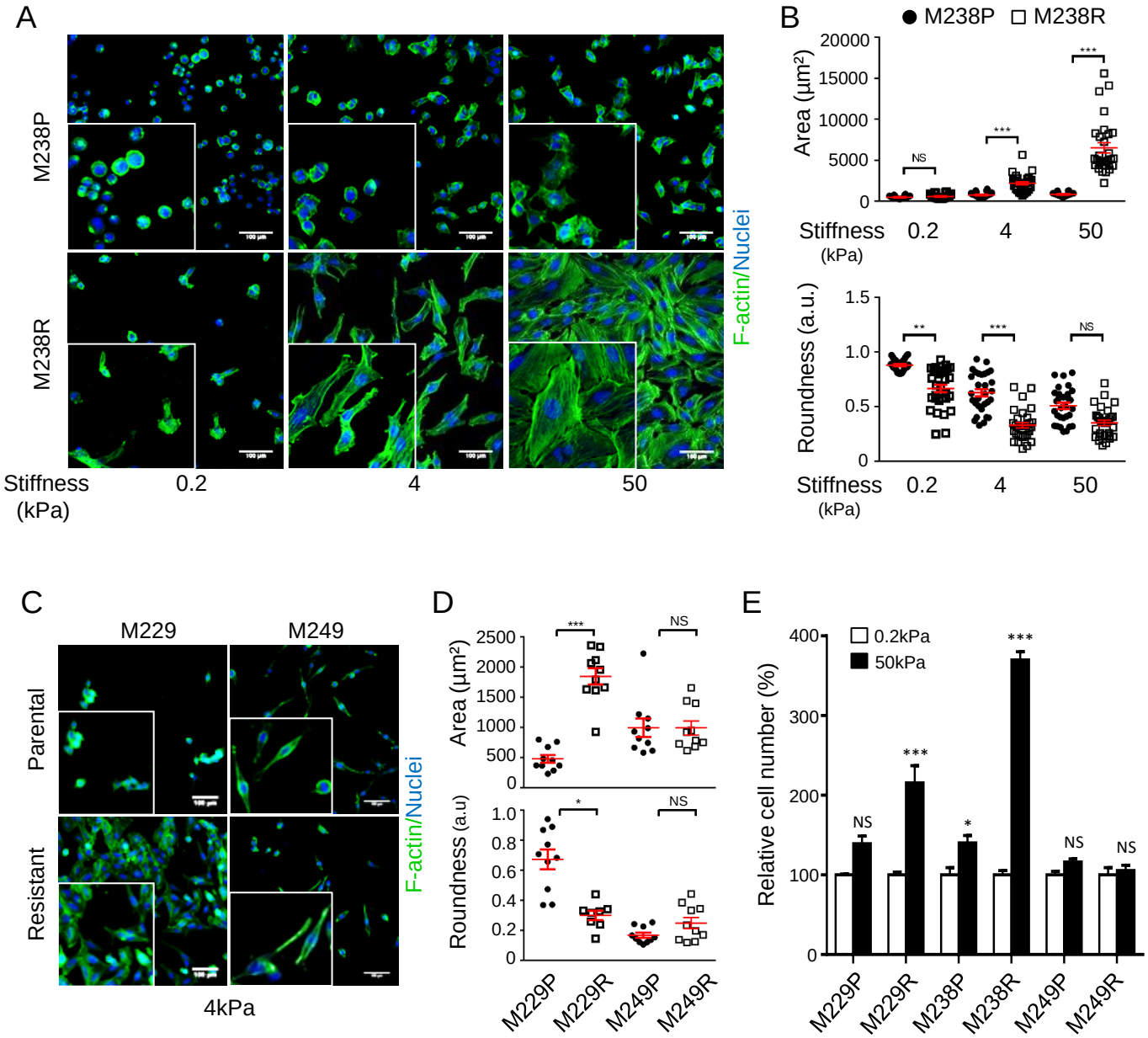
A
M238P
M238R
F-actin/Nuclei
Stiffness (kPa)
0.2
4
50
B
M238P
M238R
Area (µm²)
20000
15000
10000
5000
0
NS
***
***
Stiffness (kPa)
0.2
4
50
Roundness (a.u.)
1.5
1.0
0.5
0
**
***
NS
Stiffness (kPa)
0.2
4
50
C
M229
M249
Parental
Resistant
F-actin/Nuclei
4kPa
D
Area (µm²)
2500
2000
1500
1000
500
0
***
NS
Roundness (a.u)
1.0
0.8
0.6
0.4
0.2
0
*
NS
M229P
M229R
M249P
M249R
E
0.2kPa
50kPa
Relative cell number (%)
400
300
200
100
0
NS
***
*
***
NS
NS
M229P
M229R
M238P
M238R
M249P
M249R

Figure 2

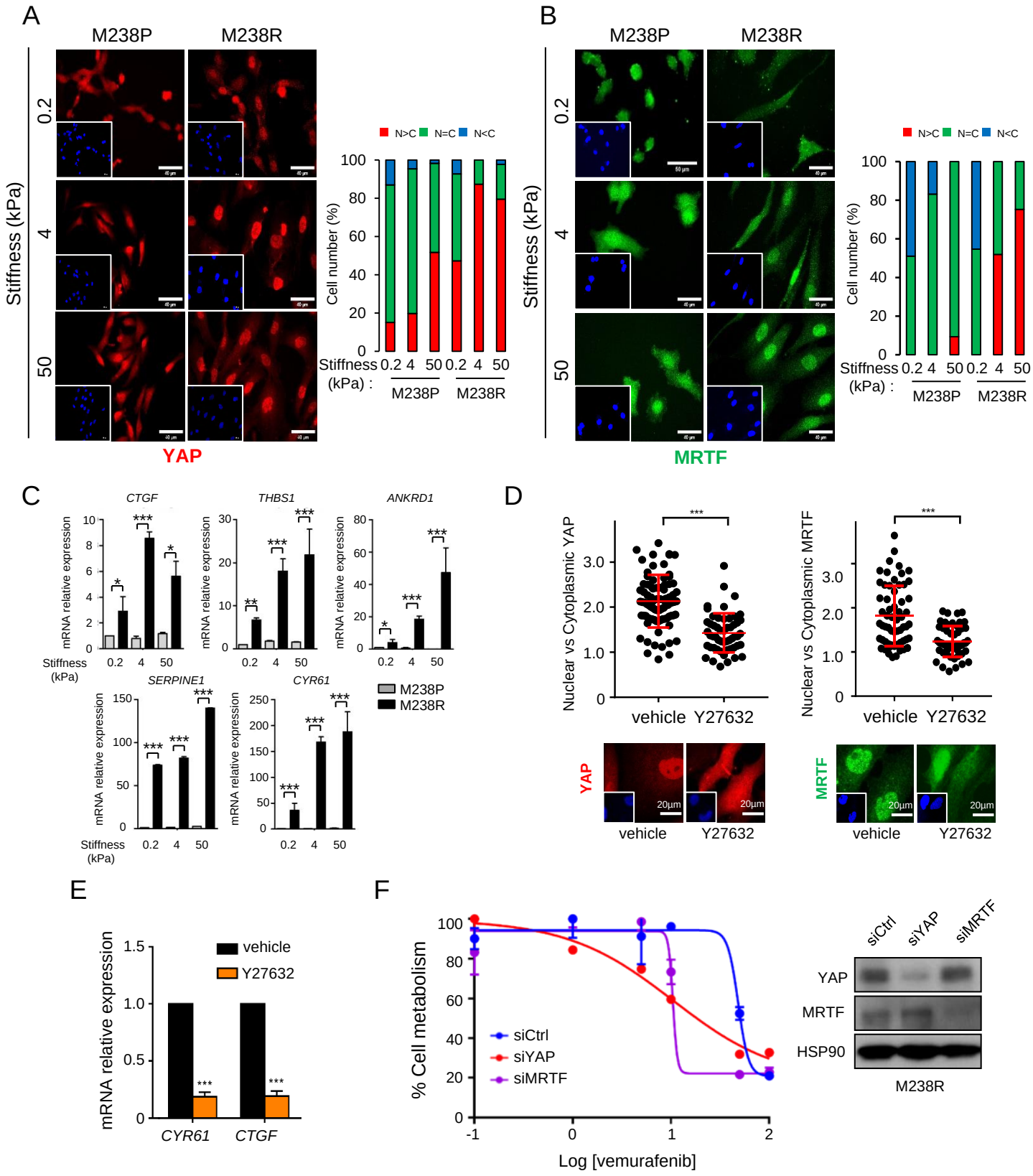
A
M238P
M238R
Stiffness (kPa)
0.2
4
50
YAP
N>C N=C N<C
Cell number (%)
Stiffness (kPa) :
0.2 4 50 0.2 4 50
M238P
M238R
B
MRTF
C
CTGF
THBS1
ANKRD1
SERPINE1
CYR61
mRNA relative expression
M238P
M238R
D
Nuclear vs Cytoplasmic YAP
Nuclear vs Cytoplasmic MRTF
vehicle
Y27632
20µm
E
mRNA relative expression
vehicle
Y27632
CYR61
CTGF
F
% Cell metabolism
siCtrl
siYAP
siMRTF
Log [vemurafenib]
HSP90
M238R

Figure 3

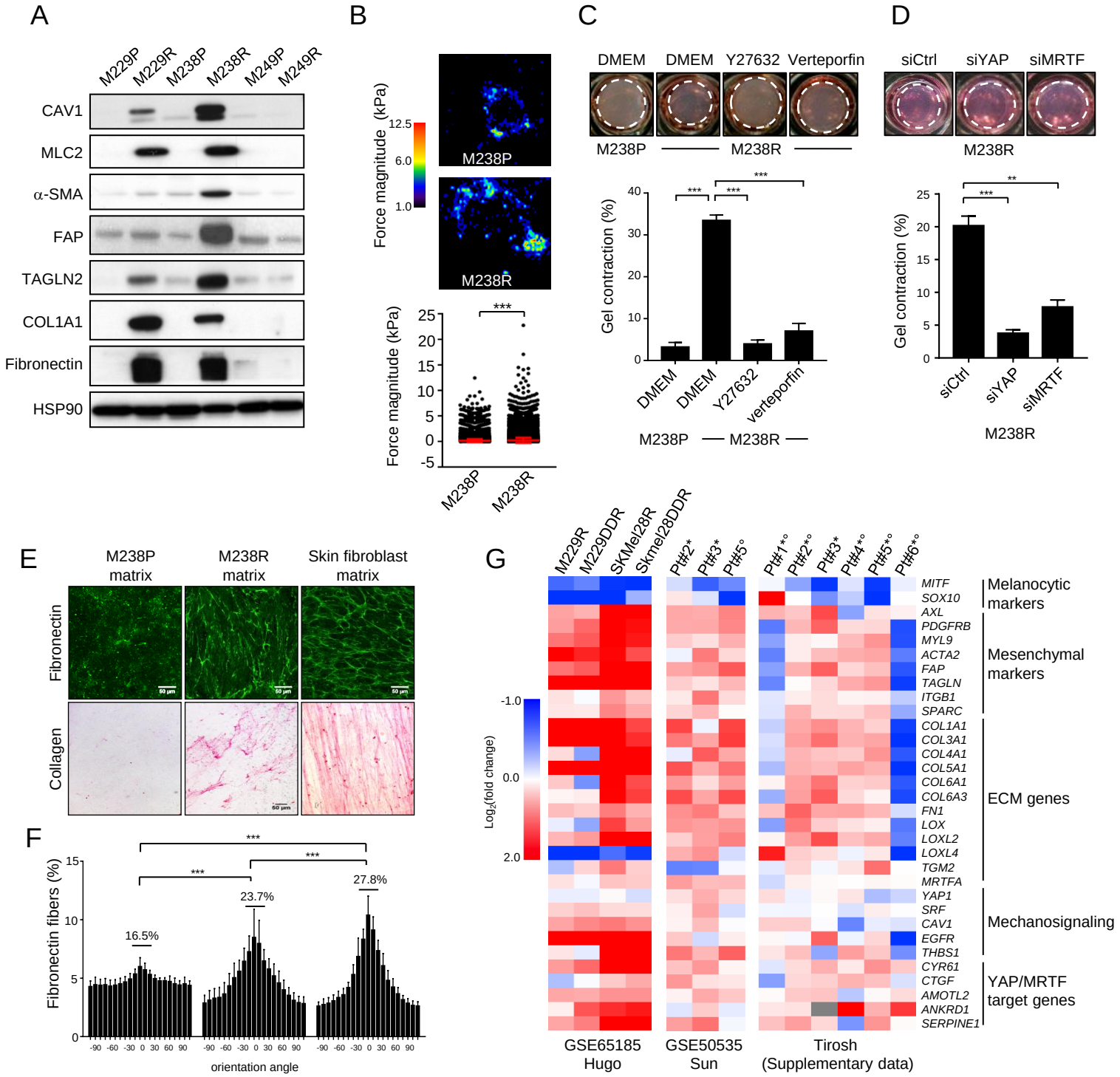
A
M229P
M229R
M238P
M238R
M249P
M249R
CAV1
MLC2
α-SMA
FAP
TAGLN2
COL1A1
Fibronectin
HSP90
B
Force magnitude (kPa)
12.5
6.0
1.0
M238P
M238R
***
Force magnitude (kPa)
M238P
M238R
C
DMEM
DMEM
Y27632
Verteporfin
M238P
M238R
Gel contraction (%)
***
***
***
DMEM
DMEM
Y27632
verteporfin
M238P
M238R
D
siCtrl
siYAP
siMRTF
M238R
Gel contraction (%)
**
***
siCtrl
siYAP
siMRTF
M238R
E
M238P matrix
M238R matrix
Skin fibroblast matrix
Fibronectin
Collagen
F
Fibronectin fibers (%)
***
***
***
16.5%
23.7%
27.8%
orientation angle
G
M229R
M229DDR
SKMel28R
Skmel28DDR
P#2*
P#3*
P#5°
P#1*°
P#2*°
P#3*
P#4*°
P#5*°
P#6*°
Log2(fold change)
-1.0
0.0
2.0
MITF
SOX10
AXL
PDGFRB
MYL9
ACTA2
FAP
TAGLN
ITGB1
SPARC
COL1A1
COL3A1
COL4A1
COL5A1
COL6A1
COL6A3
FN1
LOX
LOXL2
LOXL4
TGM2
MRTFA
YAP1
SRF
CAV1
EGFR
THBS1
CYR61
CTGF
AMOTL2
ANKRD1
SERPINE1
Melanocytic markers
Mesenchymal markers
ECM genes
Mechanosignaling
YAP/MRTF target genes
GSE65185
Hugo
GSE50535
Sun
Tirosh
(Supplementary data)

Figure 4

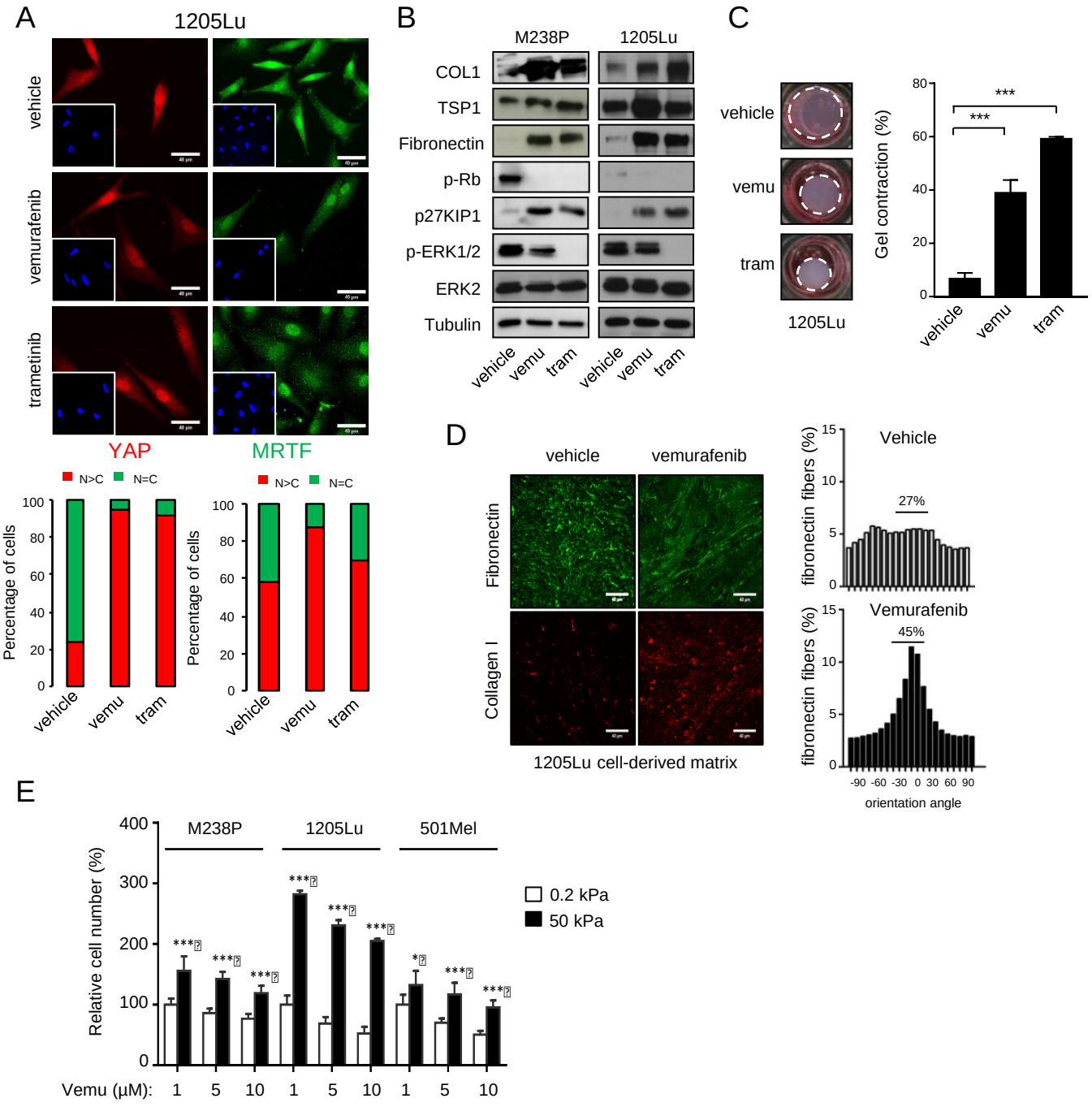
A
1205Lu
vehicle
vemurafenib
trametinib
YAP
MRTF
N>C
N=C
Percentage of cells
vehicle
vemu
tram
B
M238P
1205Lu
COL1
TSP1
Fibronectin
p-Rb
p27KIP1
p-ERK1/2
ERK2
Tubulin
C
vehicle
vemu
tram
1205Lu
Gel contraction (%)
***
D
vehicle
vemurafenib
Fibronectin
Collagen I
1205Lu cell-derived matrix
Vehicle
27%
Vemurafenib
45%
fibronectin fibers (%)
orientation angle
E
M238P
1205Lu
501Mel
Relative cell number (%)
0.2 kPa
50 kPa
Vemu (μM):

Figure 5

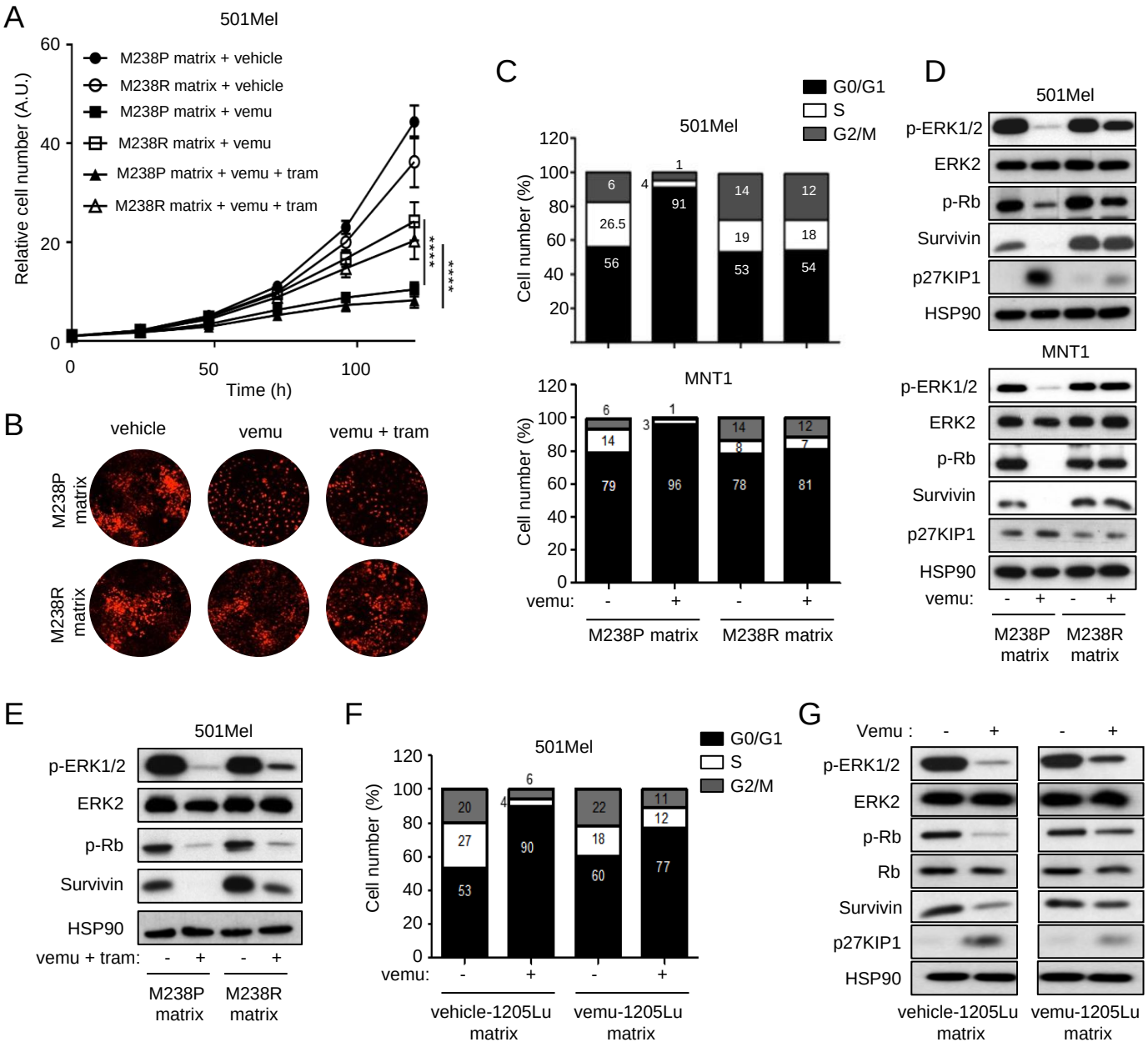
A
501Mel
M238P matrix + vehicle
M238R matrix + vehicle
M238P matrix + vemu
M238R matrix + vemu
M238P matrix + vemu + tram
M238R matrix + vemu + tram
Relative cell number (A.U.)
Time (h)
****
****
B
vehicle
vemu
vemu + tram
M238P matrix
M238R matrix
C
501Mel
MNT1
G0/G1
S
G2/M
Cell number (%)
vemu:
M238P matrix
M238R matrix
D
501Mel
MNT1
p-ERK1/2
ERK2
p-Rb
Survivin
p27KIP1
HSP90
vemu:
M238P matrix
M238R matrix
E
501Mel
p-ERK1/2
ERK2
p-Rb
Survivin
HSP90
vemu + tram:
M238P matrix
M238R matrix
F
501Mel
G0/G1
S
G2/M
Cell number (%)
vemu:
vehicle-1205Lu matrix
vemu-1205Lu matrix
G
Vemu :
p-ERK1/2
ERK2
p-Rb
Rb
Survivin
p27KIP1
HSP90
vehicle-1205Lu matrix
vemu-1205Lu matrix

Figure 6

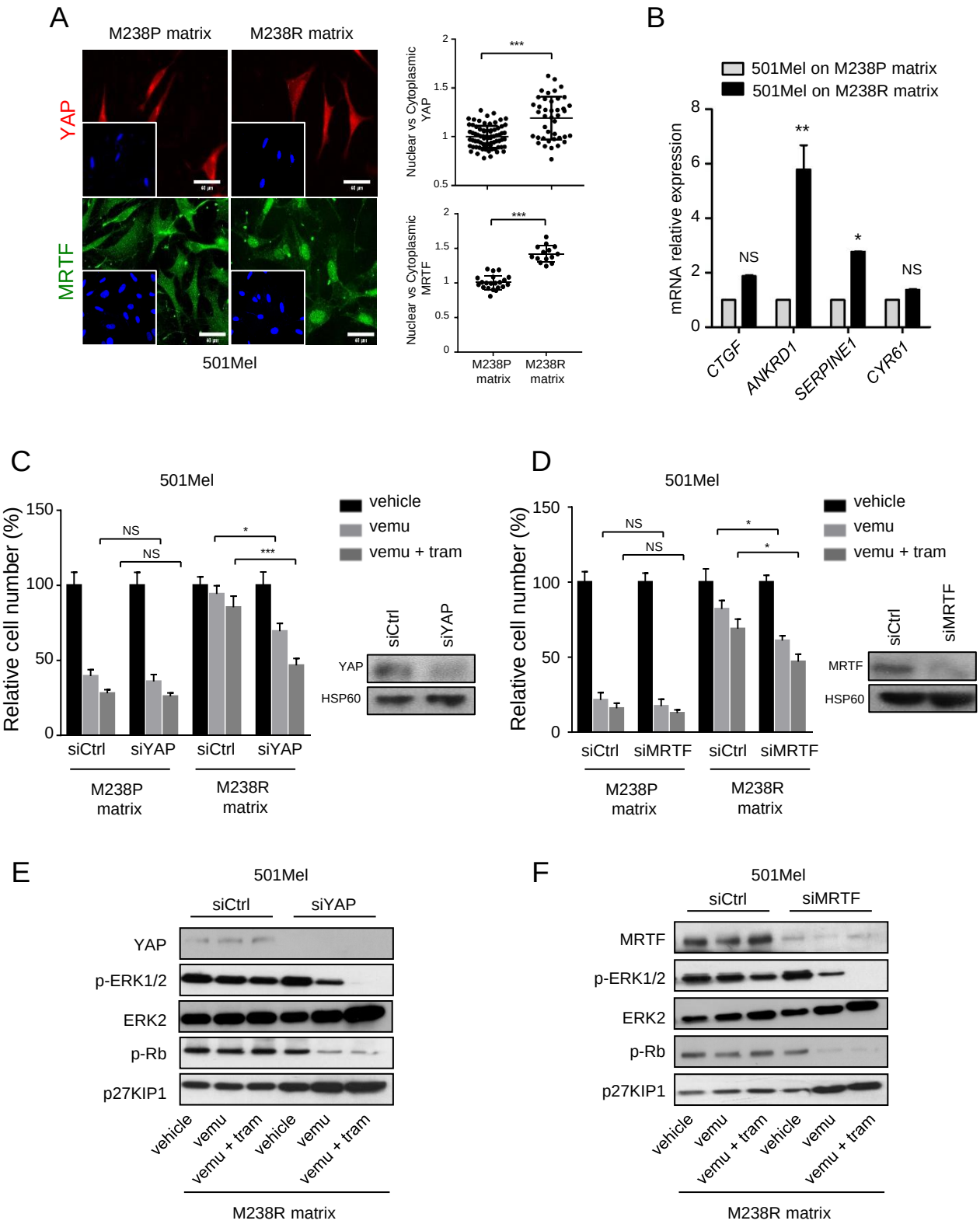
A
M238P matrix
M238R matrix
YAP
MRTF
501Mel
Nuclear vs Cytoplasmic YAP
Nuclear vs Cytoplasmic MRTF
M238P matrix
M238R matrix
B
501Mel on M238P matrix
501Mel on M238R matrix
mRNA relative expression
NS
**
*
NS
CTGF
ANKRD1
SERPINE1
CYR61
C
501Mel
Relative cell number (%)
vehicle
vemu
vemu + tram
siCtrl
siYAP
M238P matrix
M238R matrix
YAP
HSP60
D
501Mel
Relative cell number (%)
vehicle
vemu
vemu + tram
siCtrl
siMRTF
M238P matrix
M238R matrix
MRTF
HSP60
E
501Mel
siCtrl
siYAP
YAP
p-ERK1/2
ERK2
p-Rb
p27KIP1
vehicle
vemu
vemu + tram
M238R matrix
F
501Mel
siCtrl
siMRTF
MRTF
p-ERK1/2
ERK2
p-Rb
p27KIP1
vehicle
vemu
vemu + tram
M238R matrix

Figure 7

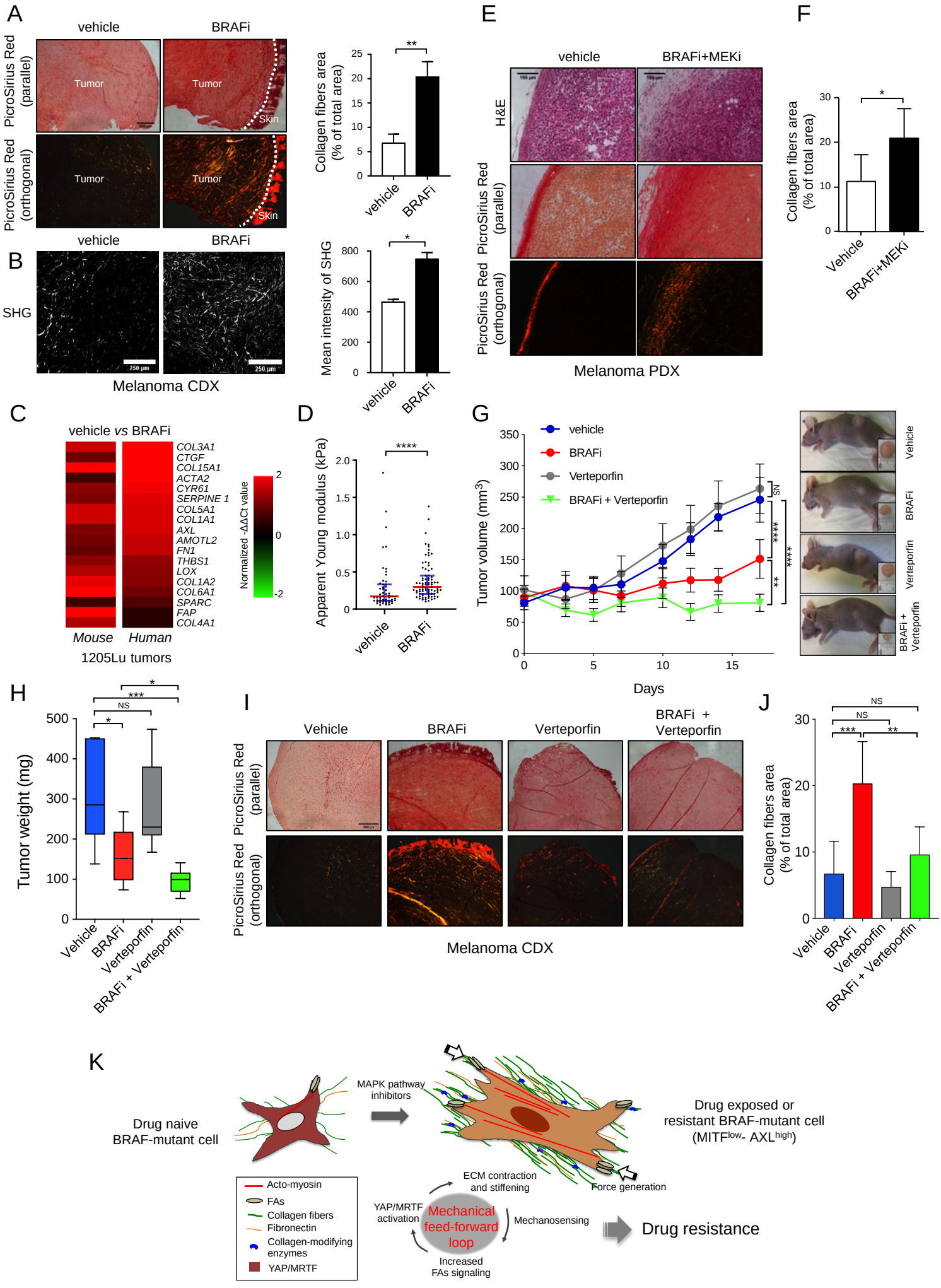
A
vehicle
BRAFi
PicroSirius Red (parallel)
PicroSirius Red (orthogonal)
Tumor
Skin
Collagen fibers area (% of total area)
B
SHG
Mean intensity of SHG
Melanoma CDX
E
H&E
vehicle
BRAFi+MEKi
Melanoma PDX
F
Collagen fibers area (% of total area)
Vehicle
BRAFi+MEKi
C
vehicle vs BRAFi
COL3A1
CTGF
COL15A1
ACTA2
CYR61
SERPINE 1
COL5A1
COL1A1
AXL
AMOTL2
FN1
THBS1
LOX
COL1A2
COL6A1
SPARC
FAP
COL4A1
Normalized -ΔΔCt value
Mouse
Human
1205Lu tumors
D
Apparent Young modulus (kPa)
G
vehicle
BRAFi
Verteporfin
BRAFi + Verteporfin
Tumor volume (mm3)
Days
H
Tumor weight (mg)
I
Vehicle
BRAFi
Verteporfin
BRAFi + Verteporfin
Melanoma CDX
J
Collagen fibers area (% of total area)
K
Drug naive BRAF-mutant cell
MAPK pathway inhibitors
Drug exposed or resistant BRAF-mutant cell (MITFlow- AXLhigh)
Acto-myosin
FAs
Collagen fibers
Fibronectin
Collagen-modifying enzymes
YAP/MRTF
ECM contraction and stiffening
Force generation
YAP/MRTF activation
Mechanical feed-forward loop
Mechanosensing
Increased FAs signaling
Drug resistance